Comparison of Extreme Coastal Flooding Events Between Tropical and Mid-Latitude Weather Systems in the Delaware and Chesapeake Bays for 1980 – 2019

John A. Callahan,[a] Daniel J. Leathers,[b] Christina L. Callahan,[b]

[a] *Delaware Geological Survey, and the Department of Geography and Spatial Sciences, University of Delaware, Newark, Delaware*

[b] *Department of Geography and Spatial Sciences, and the Center for Environmental Monitoring & Analysis, University of Delaware, Newark, Delaware*

Corresponding author: John A. Callahan, john.callahan@udel.edu

ABSTRACT

Coastal flooding is one of the most costly and deadly natural hazards facing the US Mid-Atlantic region today. Impacts in this heavily populated and economically significant region are caused by a combination of the location's exposure and natural forcing from storms and sea-level rise. Tropical cyclones (TCs) and mid-latitude (ML) weather systems each have caused extreme coastal flooding in the region. Skew surge was computed over each tidal cycle for the past 40 years (1980 – 2019) at several tide gauges in the Delaware and Chesapeake Bays to compare the meteorological component of surge for each weather type. Although TCs cause higher mean surges, ML weather systems can produce surges just as severe and occur much more frequently, peaking in the cold season (Nov – Mar). Of the top 10 largest surge events, TCs account for 30-45% in the Delaware and upper Chesapeake Bays and 40–45% in the lower Chesapeake Bay. This percentage drops to 10-15% for larger numbers of events in all regions. Mean sea-level pressure and 500 hPa geopotential height (GPH) fields of the top 10 surge events from ML weather systems show a low-pressure center west-southwest of Delmarva and a semi-stationary high-pressure center to the northeast prior to maximum surge, producing strong easterly winds. Low-pressure centers intensify under upper-level divergence as they travel eastward, and the high-pressure centers are near the GPH ridges. During lower bay events, the low-pressure centers develop further south, intensifying over warmer coastal waters, with a south-shifted GPH pattern compared to upper bay events.

1. Introduction

Although coastal storms are well-known as a multi-threat hazard along the US East Coast, bringing heavy precipitation, strong winds, large waves, and rip currents, it is coastal flooding that poses the greatest threat to human life and is often the source of much of the damage (Blake and Gibney, 2011; Rappaport, 2014; Chippy and Jawahar, 2018; Weinkle et al., 2018). The Mid-Atlantic region is especially prone to the severe impacts of coastal flooding as both economically critical human infrastructure and important natural ecosystems are found along its coasts (Sanchez et al., 2012; PDE 2017; Chesapeake Bay Program, 2020). Under current climate change model projections, mean sea levels are expected to increase globally and regionally at accelerated rates (Sweet et al., 2017b; Oppenheimer et al., 2019). Consequently, the Mid-Atlantic region's high rates of sea-level rise (SLR) (Sallenger et al., 2012; Boon et al., 2018; Piecuch et al., 2018) lead directly to increases in high-tide flood frequency (Moftakhari et al., 205; Sweet et al., 2018; Sweet et al., 2020) and in the probability of storm-based major coastal flooding events (Lin et al., 2016; Dahl et al., 2017; Rahmstorf, 2017; Garner et al., 2017; Muis et al., 2020; Taherkhani et al., 2020).

Extreme coastal flooding events can have profound negative effects as they usually include multiple hazards that compound the damage, leading to the net impact to be greater than the sum of its parts (Kopp et al., 2017; Moftakhari et al., 2017; Martzikos et al., 2021). Impacts and costs associated with coastal flooding are highly dependent upon natural and social vulnerability, the amount of exposure, and adaptation measures in place (Hallegatte et al., 2013; Hinkel et al., 2014). Varying adaptive capacity and sensitivity of coastal exposure of the wide range of land-use activities results in differing vulnerabilities across the Mid-Atlantic (Domingues et al., 2020). Local states/municipalities in this region view coastal flooding as one of the most severe and pervasive natural hazards and have been active in their

applied research and planning (Callahan et al., 2017; Boesch et al., 2018; Dupigny-Giroux et al., 2018).

Meteorologically, the Mid-Atlantic lies in a climatic transition zone between continental and marine climate types and is impacted by both tropical cyclones (TCs) and extra-tropical cyclones (ETCs) depending upon the time of year. TCs originate in the tropical and sub-tropical waters to the south-southeast from summer through mid-fall and have caused major coastal flooding to the region, most notably from Hurricanes Isabel (2003) and Sandy (2012). TCs typically bring stronger winds and higher surges but ETCs usually impact larger swaths of coastline (Pugh 2004; von Storch and Woth, 2008). ETCs that impact the Mid-Atlantic commonly originate to the west-northwest from late fall through spring. Oftentimes, they are referred to as East Coast Winter Storms, particularly when associated with snow and ice, or as nor'easters when the ETC reaches the coast and intensifies over warmer waters (Hirsch et al, 2001; Zhang et al., 2000; Thompson et al., 2013; Leathers et al., 2011). Intensification and storm track of the ETCs are often dictated by the relative position of troughs and ridges in the westerly polar jet stream. ETC low-pressure centers on the east side of upper-level troughs intensify under an area of upper-level divergence, and whose path along the coast is largely directed by upper-level ridges and nearby high-pressure systems present in the North Atlantic Ocean (Bernhardt and DeGaetano, 2012; Leathers et al., 2011). ETCs are associated with the great majority of coastal flood events in the Mid-Atlantic as compared to TCs, and those that intensify offshore (i.e., nor'easters) often follow a more meridional path, causing them to travel slower and impact the region for longer periods of time (Dolan and Davis, 1992; Zhang et al., 2000; Bernhardt and DeGaetano, 2012; Colle et al., 2015; Booth et al. 2016; Catalano and Broccoli, 2018). Some ETCs have caused damage on par with most TCs

82 in the region (DEMA, 2018), such as the Ash Wednesday Storm of 1962, the pair of
83 nor'easters in Jan-Feb 1998 (Ramsey et al., 1998), and the Mother's Day Storm of 2008.

84 Under current global warming scenarios, the frequency of major TCs, as well as their
85 wind speed and pressure center, are expected to increase in the future (Knutson et al., 2019;
86 Knutson et al., 2020), compounding the impacts from SLR alone. However, future
87 projections of ETC development and storm track position, and similarly for landfalling TCs,
88 due to changing synoptic atmospheric patterns (i.e., "storminess") in the Mid-Atlantic is
89 inconclusive (Hall et al., 2016; Mawdsley and Haigh, 2016; Michaelis et al., 2017; Dupigny-
90 Giroux et al., 2018; Lin et al., 2019). It is critical that we understand the severity and
91 geographic variability of storm surge to properly assess future risk, aid in preparedness, and
92 ultimately reduce the severe impacts from coastal flooding (CCPR, 2016).

93 Although several studies have investigated the difference between TC and ETC storm
94 types on large coastal flooding events near New York City (DeGaetano 2008; Colle et al.,
95 2010; Salmun et al., 2011; Lin et al., 2012; Talke et al., 2014, Garner, 2017), very few have
96 focused within the Mid-Atlantic. Booth et al. (2016) looked at all extreme storm surge events
97 (greater than 1-year return level) at a few selected tide gauges from Portland, ME to Duck,
98 NC. They found that for large coastal flood events covering a wider coastal area, tropical
99 systems were the most likely cause, whereas for slightly less severe events and extent, the
100 relative importance of TCs decreased and ETCs increased, with higher relative frequencies of
101 TCs to the south. Wilkerson and Brubaker (2013) investigated the spatial variability of total
102 water levels (rather than storm surge) in the central and lower Chesapeake Bay from both
103 storm types. They found that central bay gauges spent more time over the typical tidal datum
104 thresholds but had lower overall magnitudes, however, their study included only a small set
105 of events (1998 – 2011) and did not analyze storm type events separately. Catalano and

106 Broccoli (2018), focusing on the large-scale influences of ETC surge events at three locations
107 covering a large swath of the US East Coast (Boston, MA; The Battery, NYC; and Sewells
108 Pt, VA), noted a higher frequency and surge magnitude of TCs toward the south. Rashid et
109 al. (2019), using a combined SLR + storm surge index based on tide gauge observations over
110 the contiguous US coastline, and Orton et al. (2016), using separate TC and ETC simulations
111 at NYC, both concluded that characteristics of coastal flooding hazards driven by the two
112 types of storms are different and suggested to consider them separately in flood risk
113 assessments.

114 This paper will expand on previous work by focusing on the spatial variability of storm
115 surge within the Delaware and Chesapeake Bays of the US Mid-Atlantic. Water levels in
116 these bays have been well monitored for several decades by high-quality, tide-gauge
117 networks, well-suited for climate studies (Holgate et al., 2013; Sweet et al., 2017a; NOAA
118 PORTS, 2020; NOAA NWLON, 2020). Extreme surge magnitude, distribution, month of
119 occurrence, and relative frequency of events between TCs and mid-latitude (ML) weather
120 systems (encompassing ETCs, high-pressure systems, and frontal systems) will be compared
121 at numerous locations within the bays. This paper will also identify top ML surge events and
122 investigate mean sea-level pressure and 500 hPa geopotential height synoptic patterns.

123 Two other aspects that contribute to the uniqueness of the current study are the use of
124 skew surge and sub-bay regionalization in this context. Skew surge is defined as the
125 difference between the maximum total water level and the maximum predicted tide level over
126 a tidal cycle, even if the observed and predicted tidal peaks are offset (i.e., skewed) from each
127 other (Pugh and Woodworth, 2014). Although it is not commonly researched, skew surge
128 arguably better represents the meteorological component of storm surge above the
129 astronomically-forced tides and tide-surge interactions (Batstone, 2013; Mawdsley and

Haigh, 2016; Williams et al., 2016; Stephens et al., 2020). Additionally, tide gauges within the study area are grouped into sub-bay regions, each consisting of 2-3 adjacent tide gauges whose surge response and total water levels are more highly correlated to each other than to non-adjacent gauges. The list of top mid-latitude surge events produced in this paper are based on ranking of average regional skew surge rather than at individual tide gauges.

Together with Callahan et al. (2021) and Callahan and Leathers (2021), these three papers provide an in-depth summary of the top surge events in the Mid-Atlantic over the period 1980 – 2019. Severe coastal flooding is a year-round threat in the region and projected to increase in magnitude and frequency. Research into the meteorological component of storm surge and its spatial variability from multiple types of weather in the Mid-Atlantic will not only improve scientific understanding, but it will also aid in public awareness, near-term emergency preparation, and long-term planning for coastal storms.

2. Study Region

a. Delaware and Chesapeake Bays

The Delaware and Chesapeake Bays, connected via the Chesapeake and Delaware (C & D) Canal, are heavily tidally influenced with freshwater inputs from the major river systems of the Delaware River, Susquehanna River, and Potomac River (Figure 1). The Delaware Bay has a classical funnel shape, with pockets of deep scour in the wider lower bay, amplifying tidal range and storm surge in the northern regions (Wong and Münchow, 1995; Lee et al., 2017; Ross et al, 2017). The Chesapeake Bay, by contrast is longer, shallower, with more dendritic tributary landscape, with the lowest tidal ranges towards the center (Zhong and Li, 2006; Lee at al., 2017; Ross et al., 2017).

153 Although coastal storms threaten the region year-round, mean water levels follow a
154 bimodal distribution with the maximum in mid-fall and secondary maximum in late spring,
155 primarily caused by periodic fluctuations in atmospheric weather systems and coastal water
156 steric effects (NOAA CO-OPS, 2020a). Summer shows the lowest mean sea levels and
157 usually the least number of coastal storms.

158 *b. Tide Gauge Selection*

159 Tide gauges selected for the current study were limited to NOAA operational tide gauges
160 within or in the immediate vicinity of the Delaware and Chesapeake Bays. Requirements
161 were that each gauge selected would have a nearly continuous record of hourly water levels
162 over a common time period, a set of harmonic constituents identified for making tidal
163 predictions, and tidal datum conversion factors to North American Vertical Datum of 1988
164 (NAVD88). Based on the available data and findings from previous research in Callahan et
165 al. (2021), 12 tide gauges and the time period 1980 – 2019 were selected. The gauges are
166 spaced approximately evenly throughout the study area to address spatial variation in storm
167 surge response. Five gauges are associated with the Delaware Bay and seven with the
168 Chesapeake Bay (Table 1). All selected gauges are part of NOAA NWLON and PORTS
169 networks.

170 In Callahan et al. (2021), cross-correlation and principal component analysis identified
171 upper and lower bay regions of tide gauges where surge and total water levels from TCs were
172 highly correlated (Figure 1). Regions are defined as the upper (PHL, RDY) and lower (LEW,
173 CAP, ATL) Delaware Bay, and the upper (BAL, ANN, CAM) and lower (SEW, KIP, WAC)
174 Chesapeake Bay. Note that the LWS gauge was not assigned to a region as the region it was
175 most closely associated with varied between the upper and lower Chesapeake Bay. Surges

were correlated more strongly between the upper (or lower) regions across the bays than between the upper and lower region within a single bay.

Table 1. NOAA tide gauges with hourly water level data covering 1980 – 2019 used in the current study. Percent of hourly data is based upon the maximum number of hours in 1980 – 2019.

Station	Code	NOAA ID	Bay	Hourly Data
Philadelphia	PHL	8545240	Delaware	99.23%
Reedy Point	RDY	8551910	Delaware	95.61%
Lewes	LEW	8557380	Delaware	99.73%
Cape May	CAP	8536110	Delaware	98.35%
Atlantic City	ATL	8534720	Delaware	98.08%
Baltimore	BAL	8574680	Chesapeake	99.66%
Annapolis	ANN	8575512	Chesapeake	98.70%
Cambridge	CAM	8571892	Chesapeake	98.84%
Lewisetta	LWS	8635750	Chesapeake	98.72%
Kiptopeke	KIP	8632200	Chesapeake	99.78%
Sewells Point	SEW	8638610	Chesapeake	100.00%
Wachapreague	WAC	8631044	Chesapeake	89.30%

3. Data and Methods

a. Water level data processing and computation of skew surge levels

Hourly and High/Low water level data were obtained from the NOAA Center for Operational Oceanographic Products and Services (NOAA CO-OPS, 2020b). Hourly data represent the observed water level on each hour (e.g., 21:00, 22:00). High/Low data represent the exact time and magnitude of each Higher-High, High, Low, and Lower-Low tidal peak. Data at each gauge were manually inspected for errors and inconsistencies. A few small data clusters (2 – 16 hours) that existed within larger periods of missing data were removed (on seven occasions across all gauges) and small data gaps of 1-2 hours (less than 10 across all gauges) were filled using linear interpolation. Table 1 lists the percent of hourly data available for analysis based upon the total number of hours in 1980 – 2019. All gauges

had greater than 95% data availability except for the gauge at WAC (89%), due to a 2.5-year period (200511 – 200804) when valid Hourly and High/Low data were unavailable.

Harmonic Analysis (HA) was performed on the hourly water levels incorporating 37 tidal constituents defined by NOAA for their official tide predictions in this region (NOAA CO-OPS, 2020c) and seven tidal constituents noted by Harris (1991) relevant for the US East Coast to determine the predicted tide levels. Computations were carried out in 1-year time intervals, or 3-year intervals if greater than one continuous month of data were missing within a year. Annual computations minimize timing errors that can lead to the leakage of tidal energy into the non-tidal residual (Merrifield et al., 2013), essentially removes the SLR trend, and minimizes inherent constituent biases when computed over long time periods resulting from changing physiographic conditions in the bays (Ross et al., 2017) or changing seasonal weather patterns that largely affect the Sa (solar annual) and SSa (solar semi-annual) constituents (NOAA CO-OPS, 2007). Skew surge was then computed as the difference between the maximum observed total water level (TWL) from the High/Low data, and the maximum predicted tide level over each tidal cycle, even if the observed and predicted tidal peaks are offset (i.e., skewed) from each other (Pugh and Woodworth, 2014). More details on the computation of skew surge can be found in Callahan et al. (2021).

Skew surge and TWL were then detrended about the 1980-2019 mean for each gauge. Total count was a maximum of 28,231 tidal peaks over the full study time period less any missing data. All gauges showed statistically significant positive trends in TWL, whereas no gauges showed statistically significant trends in skew surge except for PHL, which showed a slight negative trend. In order to better compare magnitudes of storm-based flood levels at gauges with differing mean sea levels and tidal ranges, the skew surge time series was normalized (i.e., difference from the mean divided by standard deviation), resulting in a skew

surge index (SSI) value for each tidal cycle. Tidal peaks during major coastal flooding events were also temporally declustered to focus on the event rather than on individual high tide peaks. If multiple tidal peaks were above a selected water level threshold and within 30 hours of each other, they were treated as a single event and only the maximum value was chosen, ensuring at least two consecutive high tides between each event. Although ETCs can impact the region over multiple days, it is rare for a single system to cause multiple extreme water levels (or extreme storm surges) separated by two consecutive high tides that are both under an extreme threshold. A lower water level threshold would have required a longer declustering time interval.

Extreme skew surge and TWL thresholds for this study are defined as the 6-month return level (RL). For TWL, this lies approximately between NWS minor and moderate coastal flood advisory levels. Although this choice was arbitrary, the twice per year event could reasonably be considered extreme while still yielding enough data points (approximately 80 events over 40 years) for statistical analysis. Return levels were estimated through traditional extreme value analysis on the detrended skew surge and TWL time series using the Points-Over-Threshold (POT) sampling and fitting the exceedances to the Generalized Pareto (GP) distribution. To perform extreme value analysis using the POT/GP approach, a threshold must first be chosen that would include enough upper tail exceedances to improve the robustness of the model but not too many exceedances such that the lower exceedances introduce bias from the parent distribution. This threshold was determined separately for each tide gauge following the sequential hypothesis testing methodology described in Callahan and Leathers (2021). Thresholds for skew surge were tested for percentages ranging from 90.0 – 99.5% in 0.5% increments, whereas for TWL, the range was 95.0 – 99.5% as GP model fits using lower percentages (i.e., higher number of exceedances) failed to converge

when estimating model parameters. Once a threshold was chosen, model parameters were estimated and the 6-month RL extracted at each gauge. The 6-month RLs were compared to the Mean-Higher High Water (MHHW) and Mean Sea Level (MSL) tidal datums and their spatial variation. Since the tidal datums were computed over the National Tidal Datum Epoch (NTDE) of 1983 – 2001, these datums were adjusted by adding the difference in mean TWL over the NTDE and the study period. The adjustments were small, ranging only from 0.03 to 0.05 m across the study area.

b. Storm Type Identification

To identify if a coastal flood event was caused by a TC or ML weather system, timing of the tidal peaks was compared to storm information in the International Best Track Archive for Climate Stewardship (IBTrACS) North Atlantic Basin dataset Version 4 (Knapp et al., 2018). Systems in IBTrACS achieved a tropical cyclone classification (e.g., tropical depression, tropical storm, hurricane, sub-tropical depression, sub-tropical storm) at some point in its lifetime. Callahan et al. (2021) identified a subset of tropical cyclones in IBTrACS over the period 1980 – 2019 that impacted water levels in the Delaware and Chesapeake Bays. Note that all storm systems in IBTrACS are considered TCs for the current study, even if it transitioned to an ETC near the Delmarva Peninsula. For each TC, a time window was determined encapsulating the maximum water level and surge at each tide gauge. If a TC time window encompassed a coastal flooding event (assigned as the time of the maximum predicted tidal peak that skew surge was computed), that coastal flooding event was designated as TC, else it was designated as ML.

c. Comparison of skew surge and TWL between storm types

263 Extreme coastal flood events for TC and ML weather systems were compared in several
264 ways. Mean surge and TWL were computed at each tide gauge and tested for differences
265 using a two-sample t-test. Variances of the distribution were also computed although were
266 not quantitatively tested due to small sample size of TC events. The month of occurrence for
267 each coastal flood event was extracted and seasonal distribution at each gauge was compared
268 between weather system types.

269 The relative frequency of TCs (and therefore by contrast, of ML systems) was computed
270 for sequential numbers of top events, in multiples of five up to 100, for both surge and TWL
271 at each gauge. For example, using the ranked list of all surge events at the LEW gauge, the
272 percentage of TCs occurring within the top five events was computed. This process was
273 repeated for the top 10, top 15…, up to the top 100 events. Events ranked 80 – 100 generally
274 had lower water levels than the 6-month RL although this did not impact any results.
275 Percentages were then averaged over all gauges within each of the four regions.

276 *d. Top mid-latitude skew surge events*

277 Extreme surge events caused by ML weather systems were then investigated. Regional
278 skew surge index values were computed by averaging the tide gauge SSIs over all gauges
279 within each region for each ML extreme surge event, then ranked to generate a list of top ML
280 surge events for each region. This is the same approach taken by Callahan et al. (2021) to
281 generate a list of top TC regional surge events. A requirement for the current study is that the
282 surge must have reached at least the 6-month RL at 2 of the 3 gauges within each region for it
283 to be included as a regional extreme event. On only six occasions (4 at WAC, 1 at CAP, 1 at
284 ANN) data were not available at the third gauge, none of which were ranked in the top 10.
285 Booth et al. (2016) also took a multisite approach when determining large surge events over

an area from Massachusetts to Virginia. For the upper Delaware Bay region, surge must reach at least the 6-month RL at either one of the two gauges.

Lastly, mean composites were generated of sea level pressure (SLP) and 500 hPa geopotential height (GPH) fields of the top 10 ML surge events. Modeled data were obtained from the National Centers for Environmental Prediction (NCEP) North American Regional Reanalysis (NARR) project, a long-term (1979 – present), dynamically consistent, high-resolution, high-frequency, atmospheric and land surface hydrology dataset for the North American domain (Mesinger et al., 2006). Mean composites were produced from the 3-hourly, 0.3° gridded data product for 24 hours prior (Day-1) to 24 hours after (Day+1) the event, using the earliest time of maximum surge peak over all tide gauges within that region as the event time (Day 0). Following Colle et al. (2010) and Catalano and Broccoli (2018), the 3-hourly modeled output (e.g., 00, 03, 06 UTC, …, 21 UTC) just prior to the event time was used. For display purposes, contours were generated at 1 hPa and 25 m intervals for the SLP and 500 hPa GPH fields, respectively, after applying a 3x3 smoothing to the gridded data. Fields were compared between regions to associate the differences in synoptic meteorological conditions to differences in ML surge response.

The harmonic analysis was performed using the U-Tide package (Codiga, 2011) in the Matlab programming environment. Other tidal data analysis and comparison of weather systems was also performed in Matlab. Temporal declustering was performed using the *POT* package (Ribatet and Dutang, 2019) and the extreme value model fitting and RL extraction were performed using the *eva* package (Bader, 2020) in the R statistical computing software environment. NARR model data provided by the NOAA/OAR/ESRL PSL, Boulder, Colorado, USA from their website at https://psl.noaa.gov/data/gridded/data.narr.html.

4. Results and Discussion

a. Extreme value analysis of 6-month Return Levels

To compare extreme surges and TWL between weather systems, the 6-month RL was first extracted using POT/GP extreme value analysis after an appropriate threshold was selected, above which all of the exceedances were used to fit the GP distribution. Testing resulted in optimum threshold percentages of the surge distribution ranging from 93.5% at CAP to 99% at LEW, ANN, KIP, and SEW with no obvious spatial pattern. Testing on the TWL distribution resulted in optimum threshold percentages ranging from 95.5 – 97.0% at gauges within the lower bays and 97.5 – 99.5% in the upper bays.

TWL 6-month RLs in the Delaware Bay upper regions are larger than in its lower regions, whereas the reverse pattern holds for the Chesapeake Bay (Figure 2). Overall largest values are found in the upper Delaware Bay (maximum of 1.66 m at PHL) and the smallest values in the central-to-upper Chesapeake Bay (minimums of 0.69 and 0.70 m at LWS and ANN, respectively.) Spatial pattern of the TWL 6-month RL matches that of the MHHW tidal datum as expected since areas with high MHHW also experience the largest tidal ranges and more easily reach the 6-month RL without the need for a major storm.

Surges (particularly measured as skew surges) in this region have much less spatial variation than tidally-influenced TWL. The surge 6-month RLs range from 0.44 m at RDY to 0.59 m at LEW and ATL. Values in the central regions of each bay tend to be smaller than the upper and lower regions. Largest values are found along the open ocean coast and on the southwest inside the lower bays. These locations are more directly impacted by onshore east-northeast winds from coastal storms, which build up water from local winds and increased

volume of water into the bays form Ekman transport (due to southwest traveling ocean currents along the shoreline) and remote wind-driven surges.

Confidence intervals (CI) of the 6-month RLs are consistently narrow at all sites for both surge and TWL, driven by the large number of data points with small variance used to fit the GP model. For comparison, TWL RLs for 1 to 100-year return periods were computed (not shown) and compared against USACE (2014) as a test of the POT/GP approach. For the seven tide gauges analyzed in both studies (LEW, CAP, ATL, BAL, ANN, CAM, SEW), results matched well with differences of 0.02 – 0.06 m. Events with surge and TWL greater than the 6-month RL are defined as extreme for the remaining analysis in this paper.

b. Mean and distribution

Means of extreme surge are higher for TCs than for ML weather systems at all gauges (Table 2). Nine out of the 12 gauges (all except LEW, CAP, and WAC) show the difference to be statistically significant at the $\alpha = 0.05$ level. TC counts are relatively small, ranging from 8 at RDY and CAM to 20 at SEW, approximately 3 to 6 times smaller than ML weather system counts. Largest differences are generally in the upper bays, which support results in Callahan et al. (2021) showing most TCs stay to the south and east of Delmarva causing larger surge response in the lower bays. The upper Chesapeake Bay shows the largest mean difference although the Hurricane Isabel outlier is likely exaggerating the statistical significance. For extreme TWL events, the patterns of smaller TC frequency and higher means are generally the same as it is for surge. Differences in the means are statistically significant at ATL in the Delaware Bay and at all sites (except WAC) in the Chesapeake Bay at the $\alpha = 0.05$ level.

Table 2. Mean skew surge and total water level of extreme events caused by tropical cyclones and mid-latitude weather systems over the time period 1980 – 2019. Extreme events defined as greater than the 6-month return level. P-values are the results of two-sample t-tests; *italicized* results are statistically significant at $\alpha = 0.05$ level.

	Total Water Level					**Skew Surge**				
	Tropical		**Mid-Latitude**			**Tropical**		**Mid-Latitude**		
Station	Mean	N	Mean	N	P-value	Mean	N	Mean	N	P-value
Philadelphia	1.876	8	1.796	64	0.108	0.811	9	0.682	62	*0.022*
Reedy Point	1.509	9	1.465	70	0.281	0.712	8	0.577	66	*0.013*
Lewes	1.460	11	1.392	63	0.232	0.791	14	0.765	64	0.614
Cape May	1.521	10	1.442	65	0.069	0.706	13	0.655	59	0.247
Atlantic City	1.499	8	1.345	72	*0.004*	0.894	9	0.728	75	*0.004*
Baltimore	1.039	11	0.848	71	*0.001*	0.852	9	0.645	65	*0.006*
Annapolis	0.925	13	0.785	67	*0.004*	0.721	11	0.597	68	*0.025*
Cambridge	0.946	12	0.840	68	*0.002*	0.726	8	0.586	69	*0.002*
Lewisetta	0.876	17	0.762	65	*0.001*	0.646	13	0.520	68	*0.001*
Kiptopeke	1.053	20	0.964	59	*0.011*	0.695	19	0.594	62	*0.004*
Sewells Point	1.206	23	1.110	60	*0.040*	0.818	20	0.707	60	*0.025*
Wachapreague	1.373	16	1.318	66	0.269	0.748	16	0.723	62	0.613

Median values and overall distribution shapes are similar between weather systems for surge (Figure 3) and TWL (Supplementary Figure 1), resembling the extreme GP distribution, such as all of the outliers (i.e., data points greater than 1.5 x interquartile range) extend to the positive extreme rather than toward the lower end. Although most outliers displayed in Figure 3 are from ML systems, this is primarily due to the larger number of ML events around the median, hence decreasing the interquartile range. The absolute maximum and minimum of both surge and TWL are also similar between both weather types, aside from the extreme outlier of Hurricane Isabel in the Chesapeake. ML weather systems occur much more frequently but corresponding magnitudes and the distribution of flood levels are on par with TCs.

c. Month of occurrence

Seasonal distribution of extreme surge events has a well-defined temporal pattern (Figure 4). Nearly all sites show maximum ML surge event frequency in December or

January with a significant number of events occurring throughout the cold season (Oct – Apr), except the lower Delaware Bay which decreases in March. Very few ML or TC surge events occur during the summer (Jun – Aug). TC surge events are restricted to late summer through fall (Aug – Nov), with a maximum in September at all sites except for the lower Delaware Bay, with a maximum in October. Although many more ML than TC surge events occur over the course of a year, frequencies of extreme events caused by each weather type during the fall season are similar. Early fall (Aug – Sep) tends to be more TC events whereas mid fall (Oct – Nov) tends to be more ML events.

Seasonal distribution of extreme TWL events is similar to that of surge events but is more spread out over the year, demonstrating that coastal flooding is a threat to the Mid-Atlantic during any month, except for July when very few events occur anywhere in the study area (Supplementary Figure 2). ML TWL events in the upper Delaware Bay show noticeably low counts in February, lower than what seemingly can be attributed to its smaller number of days and should be investigated further. All Chesapeake Bay sites show a maximum in Oct for ML TWL events. Upper and central regions have significantly fewer events during the winter months before a secondary peak in Mar. Combining both TC and ML TWL events for most sites show maximum occurrences in the early fall and a secondary peak in the early spring, close to the seasonal distribution of MSL (NOAA COOPS, 2020). Seasonal peaks in MSL are due to 1) the high frequency of larger TC and ML storms and thermal expansion of coastal waters (early fall peak), and 2) the high frequency of ML storms and large high tides while the Earth is near the equinox yet not too far away from perihelion (early spring peak).

While the seasonal distribution of extreme TWL events is perhaps more closely related to mean sea levels, extreme surge is better characterized by storm intensity and tidal range. ML extreme surge events peak in the winter months when MSL is at a minimum and

399 tidal ranges are large. This is consistent with many previous studies (mentioned in the
400 Introduction) on the prevalence of wintertime ETCs, pressure-gradients, and frontal systems.
401 Tidal ranges in the summer months are minimal and MSLs are average (lower bays) to above
402 average (upper bays). Lack of extreme surge events suggest the lack of strong coastal storms
403 occurring. TC extreme TWL and surge events peak in the same months and at comparable
404 frequency, suggesting extreme coastal flooding from TCs are determined by TC strength and
405 track and not tides.

406

407 *d. Relative frequency of weather systems*

408 In all regions, the relative frequency of both extreme surge and TWL events from TCs
409 decreases as the number of top events increases (Figure 5). Of the top 20 TWL events, TCs
410 cause approximately 35-45% in the Chesapeake Bay and 20-30% in the Delaware Bay. The
411 lower Chesapeake Bay experiences the largest percent of TCs, 35 – 45% in the top 10 events
412 and 30% in the top 50 events, before declining alongside the other regions. For top surge
413 events, the pattern is very similar, albeit with a few differences. The percent of TCs in the
414 Delaware Bay is higher for the top 10 surge events (30-45%) than for TWL but drops off
415 more quickly. Upper Chesapeake Bay behaves nearly identically to the Delaware Bay regions
416 whereas the lower Chesapeake Bay percent of TCs remains high, 40 – 45% in the top 10
417 events and 25% in the top 50. These percentages asymptotically decrease to about 10-15%
418 (tested out to top 200 events, not shown). From a ML perspective, the great majority of
419 extreme surge events are from ML weather systems at 55 – 70% in the top 10 events and 80 –
420 90% in the top 50 events for the Delaware Bay and upper Chesapeake Bay, and 55 – 60% in
421 the top 10 events and 75% in the top 50 events for the lower Chesapeake Bay.

Using slightly different methods and sites further south to Duck, NC, Booth et al. (2016) found very similar results of TC percentages at 20 – 60% for the top 10 events and 10 – 30% for the top 50 events, with the larger values at the more southern locations. TCs are known to impact US Southeast coasts more often than Mid-Atlantic and Northeast coasts, and Callahan et al. (2021) showed that most TCs that approached the Delmarva Peninsula stayed to the south and east, so the conceptual implications of Figure 5 were not entirely surprising. However, the quantification of the frequency of major coastal flooding events between TC and ML weather systems, particularly focused on the measure of skew surge, as well as demonstrating the differences between the upper and lower Chesapeake Bay regions, should prove useful for forecasting future risk for long-term planning and seasonal public awareness campaigns.

e. Top mid-latitude skew surge events and synoptic composites

Table 3 shows the top 20 ML surge events for each region based on the mean storm surge index. The date/time is determined by the earliest tidal peak that reached the 6-month RL of all gauges within that region. Months of occurrence align well with Figure 4, with the great majority of the top 20 events across all regions occurring in Nov – Mar and Jan as the most common for the lower bays. Some overlap of ML events does occur among regions, most often between the lower (or upper) regions across the bays. Events on 1992-01-04, 1998-02-05, 2000-01-25, and 2016-01-23 are ranked in the top 10 for both lower Delaware and Chesapeake Bay regions. Likewise, the events on 1985-02-12, 1993-11-28, and 2012-12-21 are ranked in the top 10 for both upper bay regions. However, no common events were ranked in the top 10 between the upper and lower Chesapeake Bay regions and only the 1992-12-11 event is common between the upper and lower Delaware Bay regions.

Table 3. Ranked regional surge events from mid-latitude weather systems in upper and lower Delaware and Chesapeake Bay regions over 1980 – 2019. Ranking is ordered by skew surge index (SSI), the mean of the normalized, detrended skew surges of all gauges within that region for that event. Date and time (UTC) represent the earliest tidal peak that reached the 6-month return level at gauges within region.

	Upper Delaware		Lower Delaware		Upper Chesapeake		Lower Chesapeake	
	Date	**SSI**	**Date**	**SSI**	**Date**	**SSI**	**Date**	**SSI**
1	2012-12-21 10:54	6.65	1984-03-29 10:30	6.81	1985-11-05 02:36	5.27	2009-11-12 23:18	7.75
2	1980-10-25 17:06	5.42	1994-03-03 04:30	6.70	2011-03-11 01:30	4.87	1998-02-05 08:06	7.07
3	2005-04-02 22:42	5.14	1992-01-04 12:42	6.52	1994-01-05 00:30	4.66	2000-01-25 16:54	6.04
4	1985-02-12 21:54	4.69	1996-01-08 02:00	6.34	2018-03-07 02:00	4.58	1992-01-04 12:36	5.92
5	1993-11-28 15:00	4.59	2016-01-23 12:42	6.19	2012-12-21 07:48	4.57	2009-12-19 15:42	5.91
6	1992-12-11 04:36	4.57	1992-12-11 02:12	6.19	1985-02-13 01:18	4.57	1982-10-25 09:00	5.78
7	1982-01-04 22:30	4.35	1998-02-05 08:06	6.08	1993-11-28 12:00	4.55	1987-01-02 02:54	5.49
8	2012-11-08 13:30	4.32	2017-01-23 20:36	6.02	2003-12-11 10:23	4.49	2016-01-23 12:48	5.36
9	2003-12-14 20:12	4.11	2000-01-25 15:54	5.59	2010-01-25 17:24	4.36	1991-11-10 15:42	5.30
10	2018-04-16 16:12	4.06	1995-11-14 16:42	5.48	2016-02-09 10:12	4.12	2003-04-10 19:18	5.27
11	2011-04-17 02:42	4.00	1980-10-25 14:18	5.38	2000-12-17 16:30	4.10	2010-02-06 08:06	5.17
12	2018-03-07 07:48	3.85	2017-03-14 13:18	5.36	2006-11-16 23:30	4.03	2013-03-06 21:12	5.06
13	2016-02-09 04:24	3.82	2018-03-07 16:12	5.31	2014-10-04 06:12	3.95	2015-10-04 05:54	4.99
14	2006-10-28 08:00	3.81	2013-03-06 19:00	5.26	2011-04-16 23:12	3.93	1994-03-03 05:00	4.91
15	1985-11-05 06:48	3.79	1994-01-04 06:12	5.22	1992-12-11 08:30	3.91	1987-01-22 17:48	4.90
16	1980-03-21 22:42	3.78	2002-12-25 16:48	5.11	2010-09-30 21:00	3.90	2006-11-22 14:42	4.87
17	1999-11-03 00:36	3.73	2012-12-21 07:18	5.03	2006-10-28 12:00	3.72	2017-01-23 22:54	4.72
18	1986-12-03 04:30	3.71	1985-02-12 17:36	4.97	2015-02-12 14:24	3.72	1988-04-13 10:48	4.71
19	2011-03-10 22:06	3.64	1983-02-11 23:12	4.79	2016-02-25 02:24	3.69	1998-01-28 13:36	4.67
20	2003-12-11 05:18	3.56	2012-12-27 00:30	4.73	1983-12-13 01:54	3.69	1992-12-12 14:54	4.64

Mean synoptic conditions of the top 10 ML surge events were produced for each of the four regions to investigate the dominant weather conditions that result in extreme surges. In addition to the same geomorphologic and bathymetric factors that influence tides, surges along the coast are also influenced by coastal ocean currents, atmospheric surface pressure, wind speed and wind direction relative to the orientation of the coastline, and the size and speed of the weather system (Pore 1964; Pugh 2004; von Storch and Woth, 2008; Ellis and Sherman, 2015; Martzikos et al., 2021). The exact magnitudes of characteristics near the coast (where populated communities, and hence, tide gauges are located) are dependent upon

461 the location and persistence of the large-scale synoptic patterns in place. Note the current
462 study focuses on coastal flooding events that produce the maximum peak meteorological
463 contribution to surge, not the most damaging or most impactful storm events. Although
464 maximum surges correlate well with wind strength and direction, several studies note the
465 damage caused by coastal flooding is highly dependent upon the duration of an event (Dolan
466 and Davis, 1992; Grinsted et al., 2012; Bernhardt and DeGaetano, 2012; Martzikos et al.,
467 2021) and the relationship between maximum peak skew surge and duration in the Mid-
468 Atlantic is a timely topic for future research.

469 Figures 6-7 show the SLP and GPH mean composites, respectively, for the upper and
470 lower Delaware Bay at 24 hours prior (Day-1), the same day (Day 0), and 24 hours after
471 (Day+1) the current event. A low-pressure center (with cyclonic winds) is present to the west
472 of Delmarva while a high-pressure center (with anti-cyclonic winds) exists to the northeast in
473 the days prior to the event. The presence of the semi-stationary high pressure to the north-
474 northeast likely plays a large role in the build-up to peak flood levels as it results in tight
475 pressure-gradient-driven easterly winds as the low continues to strengthen and progress
476 towards Delmarva. For the top upper bay events, the low-pressure center develops over the
477 continental mid-west and travels east-northeast, usually directly over or staying to the
478 northwest of Delmarva. Strong southeasterly winds blow up the bays increasing water levels
479 before the low-pressure center passes and winds reverse direction. For the top lower bay
480 events, the low-pressure center develops in the southeast US and travels northeast into coastal
481 waters, staying offshore as it passes Delmarva. Since the low-pressure centers for these
482 lower bay events occur more often over the warmer, less stable ocean surface than over land
483 during the cold season (Nov – Mar), the pressure deepens further with stronger cyclonic
484 winds than for the upper bay events. The maximum difference of the low-pressure centers

485 between upper and lower bays events is approximately +11 hPa and located offshore to the
486 southeast of Delmarva (Supplementary Figure 3).

487 Mean composites of GPH for all regions show troughs in the mid-west on Day-1,
488 zonally propagating eastward. Areas of upper-level divergence, between the GPH trough and
489 ridge, align with the surface low-pressure centers to enhance cyclonic development near
490 Delmarva. The GPH trough-ridge wave pattern is translated southward during top lower bay
491 events with maximum difference in heights of about 140 m (i.e., GPH for lower bay events
492 are 140 m shallower than for upper bay events) located off the Southeast coast. Due to space
493 limitations for this paper, mean composite maps for the Chesapeake Bay events are shown in
494 Supplementary Figures 4-6. Similar spatial patterns to the Delaware Bay are exhibited for
495 Chesapeake Bay events. The Day-0 low-pressure center for upper Chesapeake Bay events is
496 elongated since some top upper Chesapeake Bay events stay further west. Intensification of
497 the low-pressure center occurs slightly further south for lower Chesapeake Bay events.

498 The GPH trough-ridge pattern and presence of the surface high-pressure in the North
499 Atlantic influences ETC storm tracks to travel in a more meridional northward pattern. Many
500 studies have correlated the atmospheric blocking patterns in the North Atlantic in the cool
501 season to more impactful and slower moving coastal storms along the US Mid-Atlantic and
502 Northeast coasts (Colle et al., 2010; Bernhardt and DeGaetano, 2012; Talke et al., 2014;
503 Catalano and Broccoli, 2018). Very similar SLP and GPH patterns were found in Leathers et
504 al. (2011) who focused on meteorologically significant events to Delmarva by analyzing
505 surface weather maps rather than tide gauge data. The combination of cyclonic low-pressure
506 centers intensifying over warmer waters under an area of upper-level divergence, traveling
507 north-northeast along the coast due to the presence of anti-cyclonic high-pressure center to
508 the northeast makes for ripe conditions for strong, long-lasting storms in the Mid-Atlantic.

509 The setup is more prominent for the top 10 lower bay events and resulted in higher SSI
510 values for the lower regions (6.19 and 5.19) compared to the upper regions (4.79 and 4.60) in
511 the Delaware and Chesapeake Bays, respectively.

512

513 ## 5. Conclusion

514 The scope of this study was to investigate the mean magnitude, distribution, time of
515 year, and synoptic conditions (for ML events) of extreme coastal flooding events in the US
516 Mid-Atlantic region over the past 40 years (1980 – 2019). Analysis was performed on
517 detrended TWL and surge values to account for SLR and other phenomena that would result
518 in near-linear changes to water levels. This time period was the longest possible to adequately
519 address the spatial variation within the Delaware and Chesapeake Bays based on tide gauge
520 data availability. However, this study did not specifically address the temporal variations.
521 Changes in the atmospheric circulation patterns (i.e., teleconnections) throughout the Western
522 Northern Hemisphere can alter storm tracks and ultimately coastal flood levels along the
523 Mid-Atlantic. Mean SLP and GPH patterns found in this study are typical of the negative
524 phase of the North Atlantic Oscillation (NAO), a measure of the difference in the semi-
525 permanent SLP regions of the Icelandic Low and Azores High. Several studies have
526 correlated the negative phase of the NAO, as well as the presence of El Niño or La Niña, to
527 increased frequency of coastal storms and flood events (Sweet and Zervas, 2011; Bernhardt
528 and DeGaetano, 2012; Thompson et al., 2013; Sweet et al., 2014; Talke et al., 2014; Sweet et
529 al., 2020). Connections are more commonly found with increased frequency of coastal
530 flooding rather than with the magnitude of surge levels. Some studies have also found more
531 complex relationships between coastal flood levels and multiple simultaneous atmospheric
532 and oceanic oscillations (Ezer et al., 2013; Hamlington et al., 2015; Wahl and Chambers,

2015; Catalano and Broccoli, 2018; Kopp et al., 2019; Rashid et al., 2019; Little et al., 2019). Although the current study period was long enough to include multiple phases of many teleconnections, future research could focus on a few select gauges within the study area with much longer periods of record to better resolve temporal trend correlations, estimates of return levels, and identification of major coastal flooding events that took place before 1980, such as the Ash Wednesday Storm of 1962, still the storm of record for lower Delaware Bay coastal flood impacts.

This study assigned the "TC" designation to all cyclones in the IBTrACS database, even though some transitioned into ETCs or merged with frontal systems as they traveled through the Mid-Atlantic region. It would be difficult to ascertain the exact time of extra-tropical transition, nonetheless, if these systems were designated as ML, the frequency of TCs in top events would likely decrease, and the prevailing synoptic patterns for SLP and GPH for top ML events may not have been as clear. Additional aspects of the current study may impact the robustness of the statistical results, although are likely minor. Selection of the 6-month RL was an arbitrary threshold for identifying extreme events. Although it yields enough data points to demonstrate patterns of surge yet represents flood levels at a magnitude that warrants preparation and planning, a lower or higher choice may have resulted in different statistics of the mean and distributions of extremes. A different approach to extreme value analysis modeling, such as using time-varying covariates, may have also resulted in a different 6-month return level. Likewise, the SLP and GPH mean composite maps may have been different if we had chosen a number greater or less than 10 or had used a fixed threshold value of SSI.

555 A few key messages were identified that will improve our understanding of the
556 magnitude, spatial variation, and synoptic conditions conducive to extreme storm surges in
557 the Mid-Atlantic region.

558 1. Coastal flooding from TCs may get much of the attention, and justifiably have a
559 higher mean surge level. ML weather systems can produce flood levels just as severe
560 and occur much more frequently. Extreme ML events occur year-round (albeit rarely
561 in Jun – Aug) while extreme TC events occur primarily in Sep - Oct. Over the course
562 of the fall season, counts of extreme TC and ML flood events are approximately
563 equal, with typically more TC events in Sep and more ML events in Oct.

564 2. Within the Delaware Bay and upper Chesapeake Bay, TCs account for 30-45% of top
565 10 and 15-20% of the top 50 surge events. The lower Chesapeake Bay has a higher
566 percentage of TC surge events at 40 – 45% of the top 10 and 25% of the top 50. For
567 both TWL and surge, the percent of TCs approaches 10-15% for larger numbers of
568 events.

569 3. Top ML surge events in the upper Delaware and Chesapeake Bays have strong
570 similarities in synoptic conditions and top 10 lists. Lower regions across the bays also
571 share these similarities, more so than with the opposing region in their own bay. This
572 behavior was also found in Callahan et al. (2021) for flood responses to TCs.

573 4. Mean SLP pattern for the top ML surge events consists of a low-pressure center
574 developing to the west of Delmarva (to the south for lower bay events) and a semi-
575 stationary high-pressure center to the northeast. Strong pressure-gradient easterly
576 winds impacted the Mid-Atlantic as the low travels east and intensifies. Low-pressure
577 centers were aligned with areas of upper-level divergence and the high-pressure
578 centers with GPH ridges. Low-pressure centers during lower bay events are located

over warmer, unstable coastal waters and shifted southward compared to upper bay events.

5. This study ranked the top surge events for the upper and lower regions of the Delaware and Chesapeake Bays from ML weather systems. Callahan et al. (2021) did the same for TCs using similar methods. Results from these two papers can be combined to form a list of top regional surge events for 1980 – 2019. Although NOAA also provides lists of top coastal flooding events over longer periods of time, those are based on observed TWL (not detrended surge) and only at individual tide gauges (not regions).

Acknowledgments.

The authors would like to thank NOAA for providing a large database of water level data for public use, and the NOAA Central Library Data Imaging Project for providing high-quality and easily accessible historical weather maps. JAC would also like to thank Dr. Daniel L. Codiga, Graduate School of Oceanography, University of Rhode Island, and Dr. Richard Pawlowicz, Department of Earth, Ocean and Atmospheric Sciences, University of British Columbia, for their help in understanding the operation of U-Tide and performing harmonic analysis.

599 REFERENCES

600 Bader, B., and J. Yan, 2020: eva: Extreme Value Analysis with Goodness-of-Fit Testing.

601 Batstone, C., Lawless, M., Tawn, J., Horsburgh, K., Blackman, D., McMillan, A., D. Worth,
602 Laeger, S., and Hunt, T., 2013: A UK best-practice approach for extreme sea-level
603 analysis along complex topographic coastlines. *Ocean Engineering*, 71, 28–39,
604 http://doi.org/10.1016/j.oceaneng.2013.02.003.

605 Bernhardt, Jase E., and Arthur T. DeGaetano, 2012: Meteorological factors affecting the
606 speed of movement and related impacts of extratropical cyclones along the U.S. east
607 coast. *Natural Hazards*, 61:1463–1472, http://doi.org/10.1007/s11069-011-0078-0.

608 Blake, E. S., and E. J. Gibney, 2011: The deadliest, costliest, and most intense United States
609 tropical cyclones from 1851to 2010 (and other frequently requested hurricane facts).
610 NOAA Technical Memorandum NWS NHC-6. 49 pp.

611 Boesch, D. F., W. C. Boicourt, R. I. Cullather, T. Ezer, G. E. Galloway Jr., Z. P. Johnson, K.
612 H. Kilbourne, M. L. Kirwan, R. E. Kopp, S. Land, M. Li, W. Nardin, C. K. Sommerfield,
613 W. V. Sweet, 2018: Sea-level Rise: Projections for Maryland 2018, 27 pp. University of
614 Maryland Center for Environmental Science, Cambridge, MD.

615 Boon, John D., M. Mitchell, J. D. Loftis, and D. L. Malmquist, 2018: Anthropogenic Sea
616 Level Change: A History of Recent Trends Observed in the U.S. East, Gulf and West
617 Coast Regions, Special Report No. 467 in Applied Marine Science and Ocean
618 Engineering, prepared by Virginia Institute of Marine Science, VA, 76 pp.

619 Booth, J. F., H. E. Rider, and Y. Kushnir, 2016: Comparing hurricane and extratropical storm
620 surge for the Mid-Atlantic and Northeast Coast of the United States for 1979–2013.

621 *Environmental Research Letters*, 11, 9, 094004, http://doi.org/10.1088/1748-
622 9326/11/9/094004.

623 Callahan, John A., Daniel J. Leathers, Christina L. Callahan, 2021: Skew Surge and Storm
624 Tides of Tropical Storms in the Delaware and Chesapeake Bays for 1980- 2019.
625 EarthArXiv [Preprint]. Accessed 26 March 2021,
626 https://www.essoar.org/doi/10.1002/essoar.10506586.1.

627 Callahan, John A., and Daniel J. Leathers, 2021: Estimation of Return Levels for Extreme
628 Skew Surge Coastal Flooding Events in the Delaware and Chesapeake Bays for 1980 –
629 2019. ESSOAr [Preprint]. Accessed 26 March 2021,
630 https://www.essoar.org/doi/abs/10.1002/essoar.10506584.1.

631 Callahan, J. A., B. P. Horton, D. L. Nikitina, C. K. Sommerfield, T. E. McKenna, and D.
632 Swallow, 2017: Recommendation of Sea-Level Rise Planning Scenarios for Delaware:
633 Technical Report, prepared for Delaware Department of Natural Resources and
634 Environmental Control (DNREC) Delaware Coastal Programs. 116 pp.

635 Catalano, Arielle J., and Anthony J. Broccoli, 2018: Synoptic Characteristics of Surge-
636 Producing Extratropical Cyclones along the Northeast Coast of the United States. *Journal*
637 *of Applied Meteorology and Climatology*, 57, 171-184, http://doi.org/10.1175/JAMC-D-
638 17-0123.1.

639 [CCPR] Council on Climate Preparedness and Resilience, 2016: Opportunities to Enhance
640 the Nation's Resilience to Climate Change. 46 pp.

641 Chesapeake Bay Program, 2020: State of the Chesapeake. Accessed 18 August 2020,
642 https://www.chesapeakebay.net/state.

643 Chippy, M. R., and S. S. Jawahar, 2018: Storm Surge and its Effect-A Review on Disaster
644 Management in Coastal Areas. *Civil Engineering Research Journal*, 4, 5, 555649,
645 http://doi.org/10.19080/CERJ.2018.04.555649.

646 Codiga, D.L., 2011: Unified Tidal Analysis and Prediction Using the UTide Matlab
647 Functions. Graduate School of Oceanography, University of Rhode Island, GSO
648 Technical Report 2011-01, 60 pp.

649 Colle, B. A., K. Rojowsky, and F. Buonaito, 2010: New York City Storm Surges:
650 Climatology and an Analysis of the Wind and Cyclone Evolution. *Journal of Applied*
651 *Meteorology and Climatology*, 49, 85-100.

652 Colle, B. A., J. F. Booth, and E. K. M. Chang, 2015: A Review of Historical and Future
653 Changes of Extratropical Cyclones and Associated Impacts along the US East Coast,
654 *Current Climate Change Reports*, 1(3):125-143, http://doi.org/10.1007/s40641-015-0013-
655 7.

656 Dahl, Kristina A., Melanie F. Fitzpatrick, Erika Spanger-Siegfried, 2017: Sea level rise drives
657 increased tidal flooding frequency at tide gauges along the U.S. East and Gulf Coasts:
658 Projections for 2030 and 2045. *PLoS One*, 12, 2.

659 DeGaetano, Arthur T., 2008: Predictability of seasonal east coast winter storm surge impacts
660 with application to New York's Long Island. *Meteorological Applications*, 15, 231–242.

661 [DEMA] Delaware Emergency Management Agency, 2018: State of Delaware All-Hazard
662 Mitigation Plan. 308 pp.

663 Dolan, R., and R. Davis, 1992: An intensity scale for Atlantic coast northeast storms. *Journal*
664 *of Coastal Research*, 8, 840–853.

665 Domingues, R., K. Keller, K. Arzayus, L. Atkinson, C. Boening, E. Di Lorenzo, G. Mitchum,
666 W. Sweet, P. Thompson, and K. White, 2020: Sea Level Hot Spots from Florida to
667 Maine: Drivers, Impacts, and Adaptation. A US CLIVAR Report, 2020-2, 40 pp,
668 http://doi.org/10.5065/nk2v-pw16.

669 Dupigny-Giroux, L.A., and Coauthors, 2018: Northeast. In Impacts, Risks, and Adaptation in
670 the United States: Fourth National Climate Assessment, Volume II [Reidmiller, D.R.,
671 C.W. Avery, D.R. Easterling, K.E. Kunkel, K.L.M. Lewis, T.K. Maycock, and B.C.
672 Stewart (eds.)]. U.S. Global Change Research Program, Washington, DC, USA, pp. 669–
673 742, http://doi.org/10.7930/NCA4.2018.CH18.

674 Ellis, J. T., and D. J. Sherman, 2015: Perspectives on Coastal and Marine Hazards and
675 Disasters, in Coastal Marine Hazards, Risks, and Disasters [John F. Shroder, Jean T. Ellis,
676 and Douglas J. Sherman, eds], http://doi.org/10.1016/B978-0-12-396483-0.01001-3.

677 Ezer, Tal, Larry P. Atkinson, William B. Corlett, and Jose L. Blanco, 2013: Gulf Stream's
678 induced sea level rise and variability along the U.S. mid-Atlantic coast, *Journal of*
679 *Geophysical Research: Oceans*, 118, 2, 685-697, http://doi.org/10.1002/jgrc.20091.

680 Garner, Andra J., and Coauthors, 2017: Impact of climate change on New York City's coastal
681 flood hazard: Increasing flood heights from the preindustrial to 2300 CE. *Proceedings of*
682 *the National Academy of Science USA*, 114, 11861–11866.

683 Grinsted, Aslak, John C. Moore, and Svetlana Jevrejeva, 2012: Homogeneous record of
684 Atlantic hurricane surge threat since 1923. *PNAS*, 109, 48,
685 http://doi.org/10.1073/pnas.1209542109.

686 Hall, J.A., S. Gill, J. Obeysekera, W. Sweet, K. Knuuti, and J. Marburger, 2016: Regional
687 Sea Level Scenarios for Coastal Risk Management: Managing the Uncertainty of Future

688 Sea Level Change and Extreme Water Levels for Department of Defense Coastal Sites
689 Worldwide. U.S. Department of Defense, Strategic Environmental Research and
690 Development Program. 224 pp.

691 Hallegatte, S., C. Green, R. J. Nicholls, and J. Corfee-Morlot, 2013: Future flood losses in
692 major coastal cities. *Nature Climate Change*. 3, 802.

693 Hamlington, B. D., R. R. Leben, K.-Y. Kim, R. S. Nerem, L. P. Atkinson, and P. R.
694 Thompson, 2015: The effect of the El Niño-Southern Oscillation on U.S. regional and
695 coastal sea level, *Journal of Geophysical Research Oceans*, 120:3970– 3986,
696 http://doi.org/10.1002/2014JC010602.

697 Harris, D. L., 1991: Reproducibility of the harmonic constants. Tidal Hydrodynamics, in B.
698 P. Parker, Ed., John Wiley and Sons, 753–771.

699 Hinkel, J., and Coauthors, 2014: Coastal flood damage and adaptation costs under 21st
700 century sea-level rise. *Proceedings of the National Academy of Science USA,* 111, 3292–
701 3297.

702 Hirsch, M.E., A. T. Degaetano, and S. J. Colucci, 2001: An East Coast Winter Storm
703 Climatology. *Journal of Climate*, 14, 882-899, http://doi.org/10.1175/1520-
704 0442(2001)014<0882:AECWSC>2.0.CO;2.

705 Holgate, S. J., A. Matthews, P. L. Woodworth, L. J. Rickards, M. E. Tamisiea, E. Bradshaw,
706 P. R. Foden, K. M. Gordon, S. Jevrejeva, and J. Pugh, 2013: New Data Systems and
707 Products at the Permanent Service for Mean Sea Level. *Journal of Coastal Research*, 29,
708 3, 493 – 504, http://doi.org/10.2112/JCOASTRES-D-12-00175.1.

709 Knapp, K. R., H. J. Diamond, J. P. Kossin, M. C. Kruk, and C. J. Schreck, 2018: International
710 Best Track Archive for Climate Stewardship (IBTrACS) Project, Version 4. [North

711 Atlantic Basin since 1980]. NOAA National Centers for Environmental Information. non-
712 government domain. Accessed 18 May 2020, http://doi.org/10.25921/82ty-9e16.

713 Knutson, T., S. J. Camargo, J. C. L. Chan, K. Emanuel, C-H. Ho, J. Kossin, M. Mohapatra,
714 M. Satoh, M. Sugi, K. Walsh, and L. Wu, 2019: Tropical Cyclones and Climate Change
715 Assessment: Part I: Detection and Attribution. *Bulletin of the American Meteorological*
716 *Society*, 1987-2007.

717 Knutson, T., S. J. Camargo, J. C. L. Chan, K. Emanuel, C-H. Ho, J. Kossin, M. Mohapatra,
718 M. Satoh, M. Sugi, K. Walsh, and L. Wu, 2020: Tropical Cyclones and Climate Change
719 Assessment: Part II: Projected Response to Anthropogenic Warming. *Bulletin of the*
720 *American Meteorological Society*, E303-E322, http://doi.org/10.1175/BAMS-D-18-
721 0194.1.

722 Kopp, Robert E., Elisabeth A. Gilmore, Christopher M. Little, Jorge Lorenzo-Trueba,
723 Victoria C. Ramenzoni, and William V. Sweet, 2019: Usable Science for Managing the
724 Risks of Sea-Level Rise. *Earth's Future*, 7, 1235 – 1269,
725 http://doi.org/10.1029/2018EF001145.

726 Kopp, R.E., K. Hayhoe, D.R. Easterling, T. Hall, R. Horton, K.E. Kunkel, and A.N.
727 LeGrande, 2017: Potential surprises – compound extremes and tipping elements. In:
728 Climate Science Special Report: Fourth National Climate Assessment, Volume I
729 [Wuebbles, D.J., D.W. Fahey, K.A. Hibbard, D.J. Dokken, B.C. Stewart, and T.K.
730 Maycock (eds.)]. U.S. Global Change Research Program, Washington, DC, USA, pp.
731 411-429, http://doi.org/10.7930/J0GB227J.

732 Kopp, R. E., 2013: Does the mid-Atlantic United States sea level acceleration hot spot reflect
733 ocean dynamic variability?, *Geophysical Research Letters*, 40:3981–3985,
734 http://doi.org/10.1002/grl.50781.

735 Leathers, Daniel, J., Robert Scarborough, and David R. Legates, 2011: Delaware Coastal
736 Storm Climatology and Damage Assessment, 1871 – 2009: Final Report. Submitted to
737 Delaware Department of Natural Resources and Environmental Control, 20 pp.

738 Lee., S. B., M. Li, and F. Zhang, 2017: Impact of sea level rise on tidal range in Chesapeake
739 and Delaware Bays. *Journal of Geophysical Research: Oceans*, 122, 3917-3938,
740 http://doi.org/10.1002/2016JC012597.

741 Lin, Ning, Reza Marsooli, and Brian A. Colle, 2019: Storm surge return levels induced by
742 mid-to-late-twenty-first-century extratropical cyclones in the Northeastern United States.
743 *Climatic Change*, 154, 143-158, http://doi.org/10.1007/s10584-019-02431-8.

744 Lin, Ning, R. E. Kopp, B. P. Horton, and J. P. Donnelly, 2016: Hurricane Sandy's flood
745 frequency increasing from 1800 to 2100, *Proceedings of the National Academy of*
746 *Science*, USA, 14(33): 12071–12075, http://doi.org/10.1073/pnas.1604386113.

747 Lin, Ning, Kerry Emanuel, Michael Oppenheimer, and Erik Vanmarcke, 2012: Physically
748 based assessment of hurricane surge threat under climate change. *Nature Climate*
749 *Change*, 2, http://doi.org/10.1038/NCLIMATE1389.

750 Little, Christopher M., Aixue Hu, Chris W. Hughes, Gerard D. McCarthy, Christopher G.
751 Piecuch, Rui M. Ponte, Matthew D. Thomas, 2019: The Relationship Between U.S. East
752 Coast Sea Level and the Atlantic Meridional Overturning Circulation: A Review, *Journal*
753 *of Geophysical Research: Oceans*, 124, 9, http://doi.org/10.1029/2019JC015152.

754 Martzikos, Nikolas T., Panayotis E. Prinos, Constantine D. Memos, and Vasiliki K. Tsoukala,
755 2021: Key research issues of coastal storm analysis. *Ocean and Coastal Management*,
756 199, http://doi.org/10.1016/j.ocecoaman.2020.105389.

757 Merrifield, M. A., A. S. Genz, C. P. Kontoes, and J. J. Marra, 2013: Annual maximum water
758 levels from tide gauges: Contributing factors and geographic patterns. *Journal of*
759 *Geophysical Research: Oceans*, 118, 2535–2546, http://doi.org/10.1002/jgrc.20173.

760 Mesinger, Fedor and Coauthors, 2006: North American Regional Reanalysis. *Bulletin of the*
761 *American Meteorological Society*, 87, 3, 343 – 360, http://doi.org/10.1175/BAMS-87-3-
762 343.

763 Mawdsley, R. J., and J. D. Haigh, 2016: Spatial and Temporal Variability and Long-Term
764 Trends in Skew Surges Globally. *Frontiers in Marine Science*, 3, 1-29,
765 http://doi.org/10.3389/fmars.2016.00029.

766 Michaelis, A. C., J. Willison, G. M. Lackmann, and W. A. Robinson, 2017: Changes in
767 winter North Atlantic extratropical cyclones in high resolution regional pseudo–global
768 warming simulations. *Journal of Climate*, 30, 6905–6925.

769 Moftakhari, H. R., A. AghaKouchak, B. F. Sanders, D. L. Feldman, W. V. Sweet, R. A.
770 Matthew, and A. Luke, 2015: Increased nuisance flooding along the coasts of the United
771 States due to sea level rise: Past and future, *Geophysical Research Letters*, 42, 9846–
772 9852, http://doi.org/10.1002/2015GL066072.

773 Muis S., Irazoqui, Apecechea M., Dullaart, J., de Lima, Rego J., Madsen, K.S., Su, J., Yan,
774 K., and M. Verlaan, 2020: A High-Resolution Global Dataset of Extreme Sea Levels,
775 Tides, and Storm Surges, Including Future Projections. *Frontiers in Marine Science*,
776 7:263, http://doi.org/10.3389/fmars.2020.00263.

777 NOAA CO-OPS, 2020a: NOAA National Ocean Service Center for Operational
778 Oceanographic Products and Services (CO-OPS). Sea Level Trends. Accessed 18 August
779 2020, https://tidesandcurrents.noaa.gov/sltrends/.

780 NOAA CO-OPS, 2020b: NOAA National Ocean Service Center for Operational
781 Oceanographic Products and Services (CP-OPS). API for Data Retrieval. Accessed 9
782 April 2020, https://api.tidesandcurrents.noaa.gov/api/prod/.

783 NOAA CO-OPS, 2020c: NOAA National Ocean Service Center for Operational
784 Oceanographic Products and Services (CO-OPS). NOAA Tide Predictions. Accessed 9
785 April 2020, https://tidesandcurrents.noaa.gov/tide_predictions.html.

786 NOAA NWLON, 2020: NOAA National Ocean Service National Water Level Observation
787 Network (NWLON). Accessed 18 August 2020,
788 https://www.tidesandcurrents.noaa.gov/nwlon.html.

789 NOAA PORTS, 2020: National Ocean Service Physical Oceanographic Real-Time System
790 (PORTS). Accessed 18 August 2020, https://tidesandcurrents.noaa.gov/ports.html

791 Oppenheimer, M., B.C. Glavovic, J. Hinkel, R. van de Wal, A.K. Magnan, A. Abd-Elgawad,
792 R. Cai, M. CifuentesJara, R.M. DeConto, T. Ghosh, J. Hay, F. Isla, B. Marzeion, B.
793 Meyssignac, and Z. Sebesvari, 2019: Sea Level Rise and Implications for Low-Lying
794 Islands, Coasts and Communities. In: IPCC Special Report on the Ocean and Cryosphere
795 in a Changing Climate [H.-O. Pörtner, D.C. Roberts, V. Masson-Delmotte, P. Zhai, M.
796 Tignor, E. Poloczanska, K. Mintenbeck, A. Alegría, M. Nicolai, A. Okem, J. Petzold, B.
797 Rama, N.M. Weyer (eds.)]. In press.

798 Orton, P.M., T.M. Hall, S.A. Talke, A.F. Blumberg, N. Georgas, and S. Vinogradov, 2016:
799 A. validated tropical-extratropical flood hazard assessment for New York Harbor. *Journal*
800 *of Geophysical. Research: Oceans*, 121, no. 12, 8904-8929,
801 http://doi.org/10.1002/2016JC011679.

802 [PDE] Partnership for the Delaware Estuary, 2017: Technical Report for the Delaware
803 Estuary and Basin 2017. L. Haaf,, S. Demberger, D. Kreeger, and E. Baumbach (eds).
804 PDE Report No. 17-07. 379 pp.

805 Piecuch, C. G., P. Huybers, C. C. Hay, A. C. Kemp, C. M. Little, J. X. Mitrovica, R. M.
806 Ponte, and M. P. Tingley, 2018: Origin of spatial variation in US East Coast sea-level
807 trends during 1900–2017. *Nature*, 564, 400-404, http://doi.org/10.1038/s41586-018-
808 0787-6.

809 Pore, N. Arthur, 1964: The relation of wind and pressure to extratropical storm surge AT
810 Atlantic City. *Journal of Applied Meteorology*, 3, 155-163.

811 Pugh, David, 2004: *Changing Sea Levels: Effects of Tides, Weather, and Climate*. Cambridge
812 University Press, 265 pp.

813 Pugh, David, and Phillip Woodworth, 2014: Sea-*Level Science: Understanding Tides,*
814 *Surges, Tsunamis and Mean Sea-Level Changes*. Cambridge University Press, 395 pp.

815 Rahmstorf, S., 2017: Rising hazard of storm-surge flooding. *PNAS Commentary*, 114:45,
816 11806-11808, http://doi.org/10.1073/pnas.1715895114.

817 Ramsey, K. W., D. J. Leathers, D. V. Wells, and J. H. Talley, 1998. Summary Report: The
818 Coastal Storms of January 27-29 and February 4-6, 1998, Delaware and Maryland.
819 Delaware Geological Survey Open File Report 40, 47 pp.

820 Rappaport, E., 2014: Fatalities in the United States from Atlantic Tropical Cyclones New
821 Data and Interpretation. *Bulletin of the American Meteorological Society Insights and*
822 *Innovations*, 341 – 346.

823 Rashid, M., T. Wahl, D. Chambers, F. Calafat, and W. Sweet, 2019: An extreme sea level
824 indicator for the contiguous United States coastline, *Sci Data*, 6, 326,
825 http://doi.org/10.1038/s41597-019-0333-x.

826 Ribatet, Mathieu, and Christopher Dutang, 2019: POT: Generalized Pareto Distribution and
827 Peaks Over Threshold. R package version 1.1-7.

828 Ross, A. C., Najjar, R. G., Li, M., Lee, S. B., Zhang, F., and Liu, W., 2017: Fingerprints of
829 sea level rise on changing tides in the Chesapeake and Delaware Bays. *Journal of*
830 *Geophysical Research: Oceans*, 122, 8102–8125, http://doi.org/ 10.1002/2017JC012887.

831 Sallenger, A. H., K. S. Doran, and P. A. Howd, 2012: Hotspot of accelerated sea-level rise on
832 the Atlantic coast of North America, *Nature Climate Change*, 2, 884–888,
833 http://doi.org/10.1038/nclimate1597.

834 Salmun, H., A. Molod, K. Wisniewska, and F. S. Buonaiuto, 2011: Statistical Prediction of
835 the Storm Surge Associated with Cool-Weather Storms at the Battery, New York. *Journal*
836 *of Applied Meteorology and Climatology*, 50. 273-282.

837 Sanchez, J. R., G. Kauffman, K. Reavy, and A. Homsey, 2012: Chapter 1.7 - Natural Capital
838 Value. *Technical Report for the Delaware Estuary and Basin*. Partnership for the
839 Delaware Estuary. PDE Report No.17-07 pp. 70-75.

840 Smith, A., 2021: 2020 U.S. billion-dollar weather and climate disasters in historical context,
841 Technical Report, http://doi.org/10.13140/RG.2.2.25871.00166/1.

842 Stephens, S. A., R. G. Bell, and I. D. Haigh, 2020: Spatial and temporal analysis of extreme
843 storm-tide and skew-surge events around the coastline of New Zealand. *Natural Hazards*
844 *and Earth System Sciences*, 20, 3, 783-796.

845 Sweet, W., G. Dusek, G. Carbin, J. Marra, D. Marcy, and S. Simon, 2020: 2019 State of U.S.
846 High Tide Flooding with a 2020 Outlook. NOAA Technical Report NOS CO-OPS 092,
847 24 pp.

848 Sweet, W. V., G. Dusek, J. Obeysekera, and J. J. Marra, 2018: Patterns and Projections of
849 High Tide Flooding Along the U.S. Coastline Using a Common Impact Threshold.
850 NOAA Technical Report NOS CO-OPS 086, 56 pp.

851 Sweet, W. V., R. M. Horton, R. E. Kopp, A. N. LeGrande, and A. Romanou, 2017a: Sea level
852 rise. In: Climate Science Special Report: Fourth National Climate Assessment, Volume I
853 [Wuebbles, D.J., D.W. Fahey, K.A. Hibbard, D.J. Dokken, B.C. Stewart, and T.K.
854 Maycock (eds.)]. U.S. Global Change Research Program, Washington, DC, USA, pp.
855 333-363, http://doi.org/10.7930/J0VM49F2.

856 Sweet, W. V., R. E. Kopp, C. P. Weaver, J. Obeysekera, R. M. Horton, E. R. Thieler, and C.
857 Zervas, 2017b: Global and Regional Sea Level Rise Scenarios for the United States.
858 NOAA Technical Report NOS CO-OPS 083, 75 pp.

859 Sweet, W. V., Park, J., Marra, J. J., Zervas, C. E., and Gill, S., 2014: Sea Level Rise and
860 Nuisance Flood Frequency Changes around the United States. NOAA Technical Report
861 NOS CO-OPS 073, 66 pp.

862 Sweet, W. V., and C. Zervas, 2011: Cool-Season Sea Level Anomalies and Storm Surges
863 along the U.S. East Coast: Climatology and Comparison with the 2009/10 El Nino.
864 Monthly Weather Review, 139, 2290 – 2299, http://doi.org/10.1175/MWR-D-10-
865 05043.1.

866 Taherkhani, M., S. Vitousek, P. Barnard, N. Frazer, T. Anderson, & C. Fletcher, 2020: Sea-
867 level rise exponentially increases coastal flood frequency. *Scientific Reports*, 10.

868 Talke, S. A., P. Orton, and D. A. Ray, 2014: Increasing storm tides in New York Harbor,
869 1844–2013. *Geophysical Research Letters*, 41, 3149–3155,
870 http://doi.org/10.1002/2014GL059574.

871 Thompson, P. R., G. T. Mitchum,, C. Vonesch, and J. Li, J., 2013: Variability of Winter
872 Storminess in the Eastern United States during the Twentieth Century from Tide Gauges.
873 *Journal of Climate*, 26, 919 9713-9726, http://doi.org/10.1175/JCLI-D-12-00561.1.

874 von Storch, H., and K. Woth, 2008: Storm surges, perspectives, and options. *Sustainability*
875 *Science*, 3, 33–43, http://doi.org/10.1007/s11625-008-0044-2.

876 Wahl, Thomas V., and Don P. Chambers, 2015: Evidence for multidecadal variability in US
877 extreme sea level records. *Journal of Geophysical Research: Oceans*, 120, 1527-1544,
878 http://doi.org/ 10.1002/2014JC010443.

879 Weinkle, J., C. Landsea, D. Collins, R. Musulin, R. P. Crompton, P. K. Klotzbach, and R.
880 Pielke Jr., 2018: Normalized hurricane damage in the continental United States 1900–
881 2017. *Nature Sustainability*, http://doi.org/10.1038/s41893-018-0165-2.

882 Wilkerson, C. N., and J. Brubaker, 2013: Analysis of Extreme Water Levels in the Lower
883 Chesapeake Bay. *Proceedings of the 2012 OCEANS Conference*, Hampton Roads, VA,
884 http://doi.org/10.1109/OCEANS.2012.6405098.

885 Williams, J., K. J. Horsburgh, J. A. Williams, and R. N. F. Proctor, 2016: Tide and skew
886 surge independence: New insights for flood risk. *Geophysical Research Letters*, 43,
887 6410–6417, http://doi.org/10.1002/2016GL069522.

888 Wong, K–C., and A. Münchow, 1995: Buoyancy forced interaction between estuary and
889 inner shelf: observation. *Continental Shelf Research*, 15, 1, 59-88.

890 Zhang, K., B. C. Douglas, and S. P. Leatherman, S. P., 2000: Twentieth-Century Storm
891 Activity along 944 the U.S. East Coast. *Journal of Climate*, 13, 1748-1761.
892 Zhong, L., and M. Li, 2006: Tidal Energy Fluxes and Dissipation in the Chesapeake Bay.
893 *Continental Shelf Research*, 26, 6, 752-770.
894
895

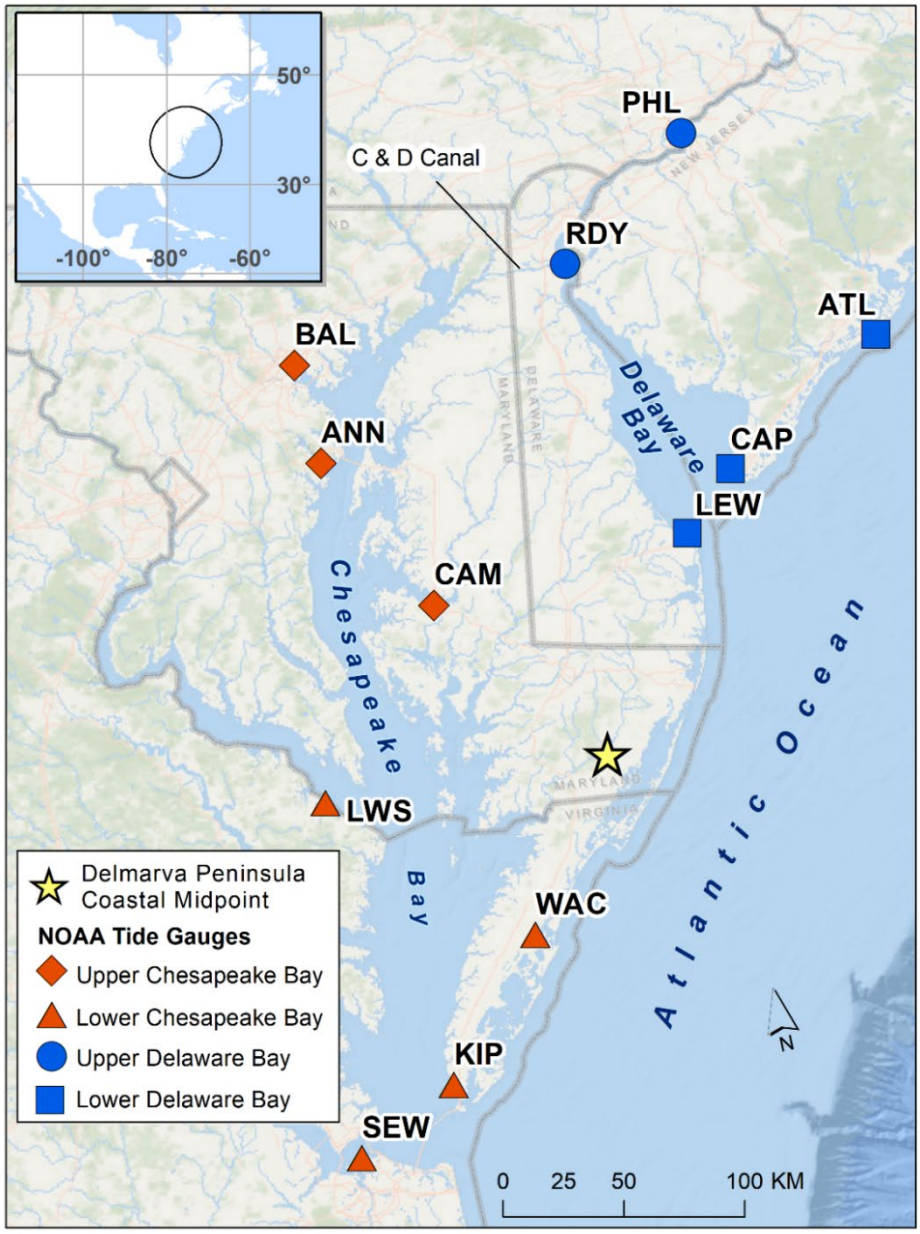

Figure 1. Map of the Delaware and Chesapeake Bays with the 12 NOAA tide gauges used in the current study: Philadelphia (PHL), Reedy Point (RDY), Cape May (CAP), Atlantic City (ATL), Baltimore (BAL), Annapolis (ANN), Cambridge (CAM), Lewisetta (LWS), Kiptopeke (KIP), Sewells Point (SEW), Wachapreague (WAC). Figure adapted from Callahan et al. (2021).

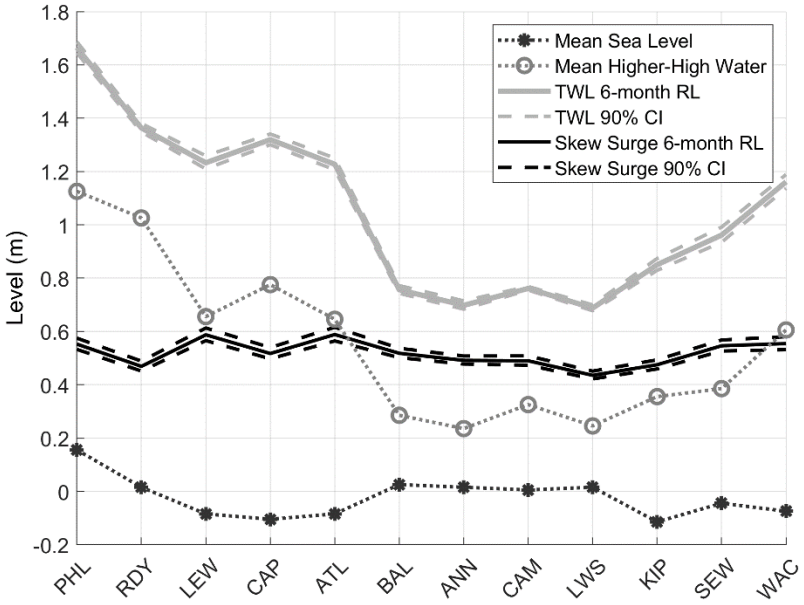

Figure 2. Surge and total water level with 90% confidence intervals (CI) for 6-month return level (RL) over 1980 – 2019. Mean Higher-High Water and Mean Sea Level tidal datums published by NOAA over the 1983-2001 National Tidal Datum Epoch.

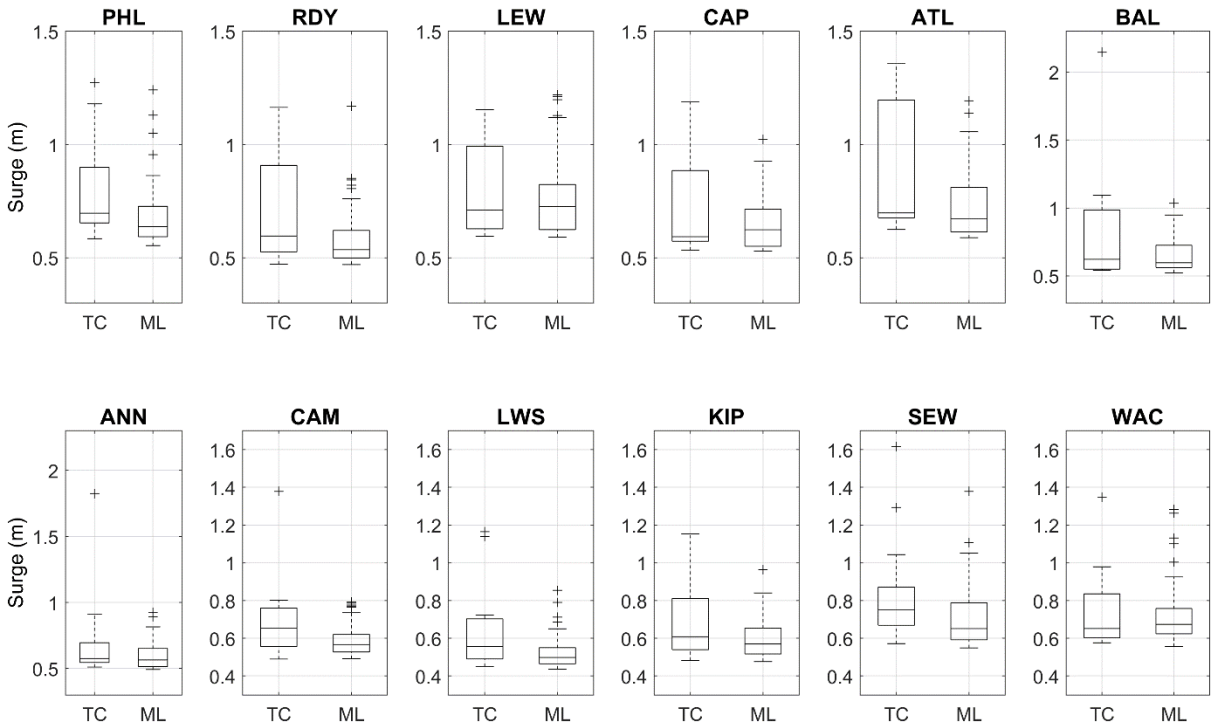

Figure 3. Distributions of extreme surge due to tropical cyclones (TC) and mid-latitude (ML) weather systems over 1980 – 2019. Extreme levels defined as greater than 6-month return level. Box plots show medians, interquartile ranges (rectangular box), and maximum/minimum values (hash marks) that are not considered outliers. Outliers represent data greater than 1.5 times interquartile range.

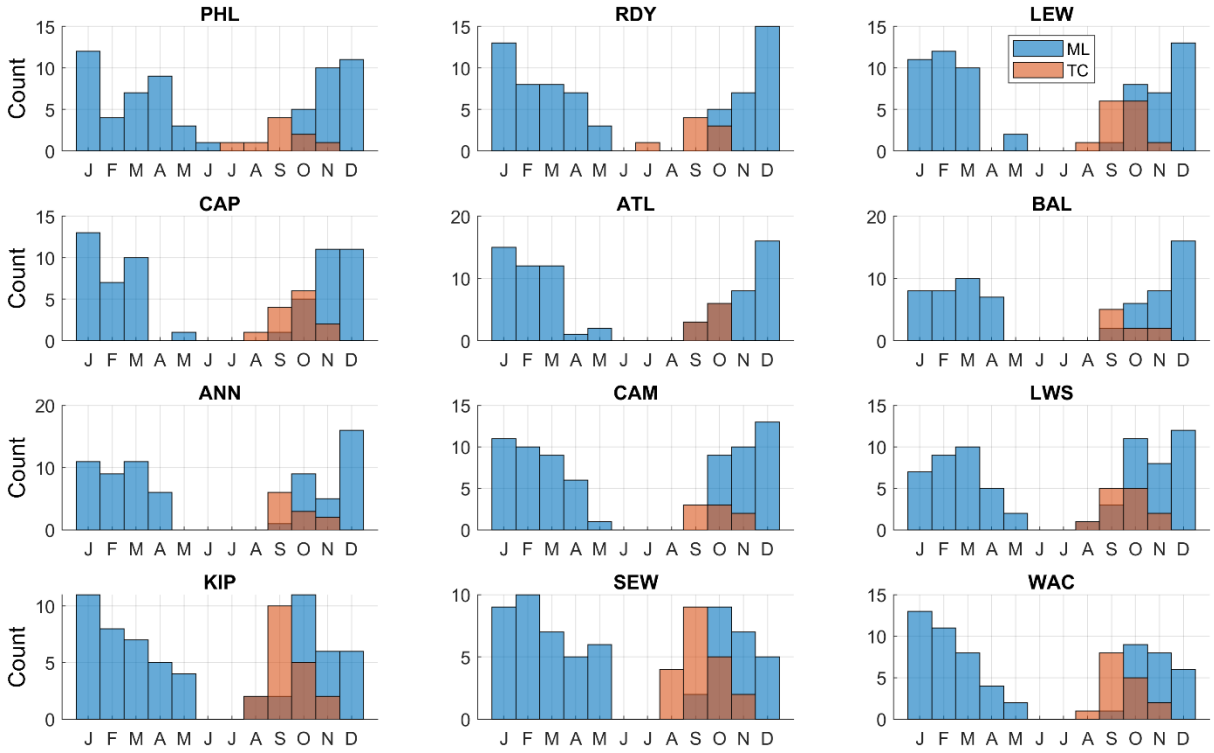

Figure 4. Monthly frequency of occurrences of extreme surge events due to tropical cyclones (TC, orange bars) and mid-latitude (ML, blue bars) weather systems over 1980 – 2019. Extreme levels defined as greater than 6-month return level.

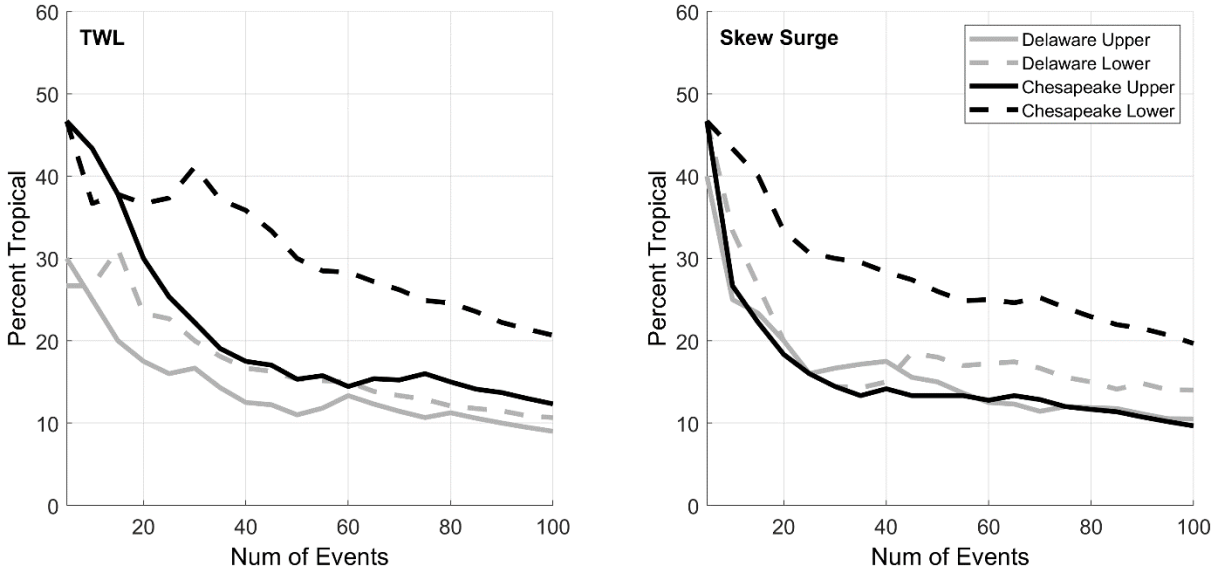

936
937
938
939 **Figure 5.** Frequency of tropical cyclones of ranked total water level (TWL) and surge events for
940 regions within the Delaware (grey) and Chesapeake (black) Bays over 1980 – 2019. Solid lines
941 represent the upper bay regions and dashed lines represent the lower bay regions.

942
943
944

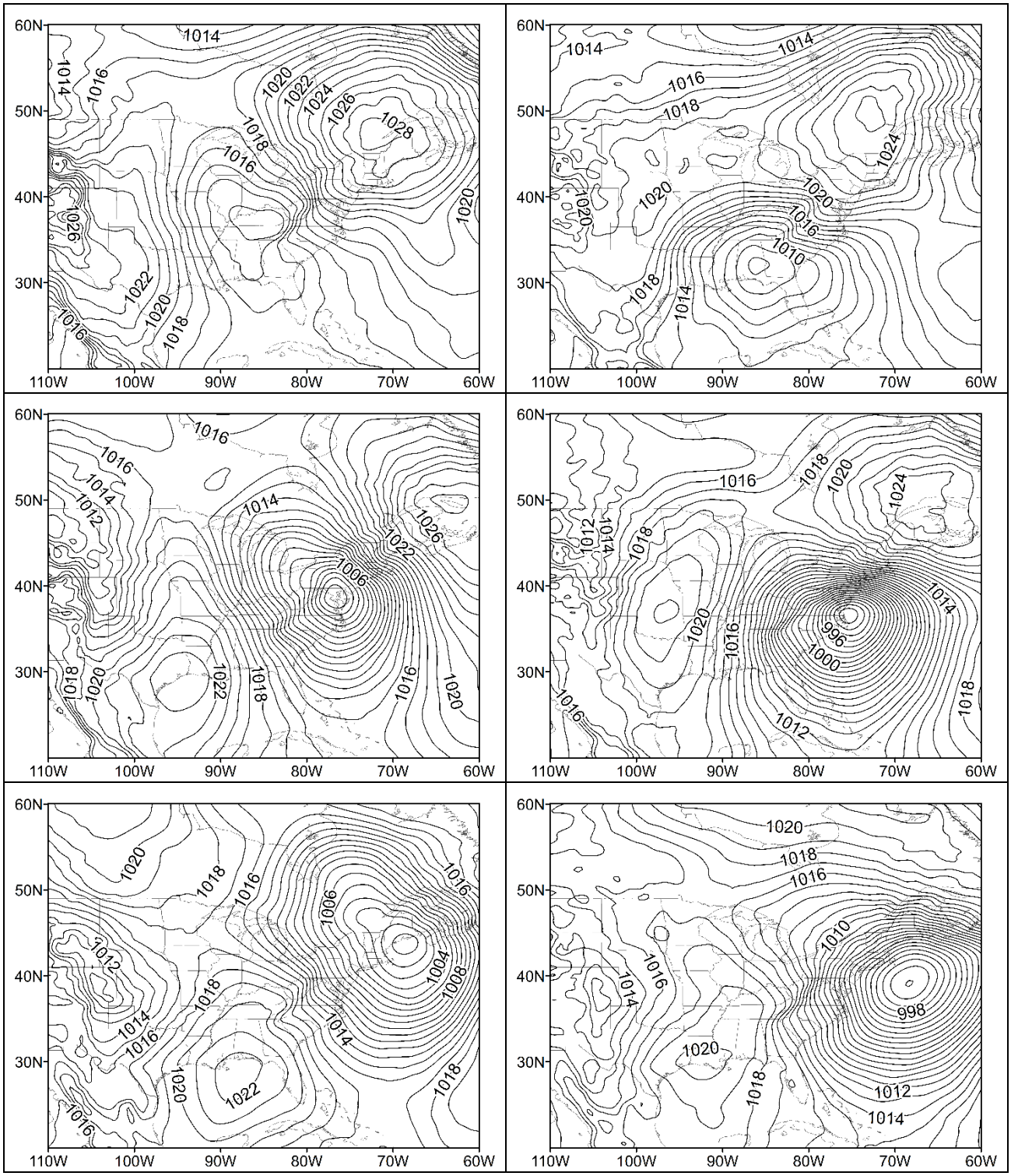

945
946 **Figure 6.** Mean sea-level pressure composite maps of top 10 surge events caused by mid-latitude
947 weather systems, for 24 hours before the event (top row), day of the event (middle row), and 24 hours
948 after the event (bottom row). Left (right) column the upper (lower) Delaware Bay. Data from North
949 American Regional Reanalysis project.

950
951
952

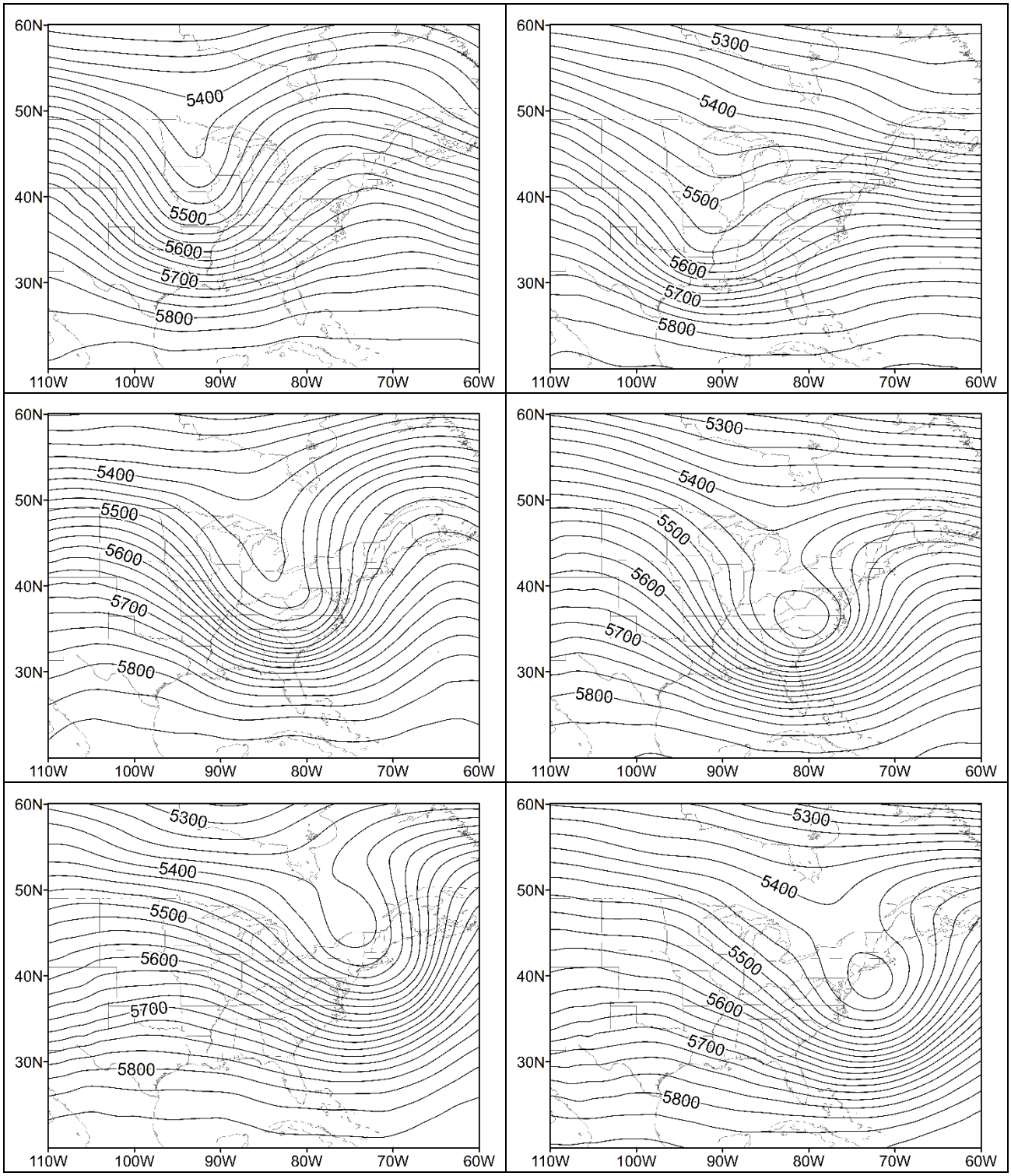

Figure 7. Mean 500 hPa geopotential height composite maps of top 10 surge events caused by mid-latitude weather systems, for 24 hours before the event (top row), day of the event (middle row), and 24 hours after the event (bottom row). Left (right) column the upper (lower) Delaware Bay. Data from North American Regional Reanalysis project.

Supplementary Materials

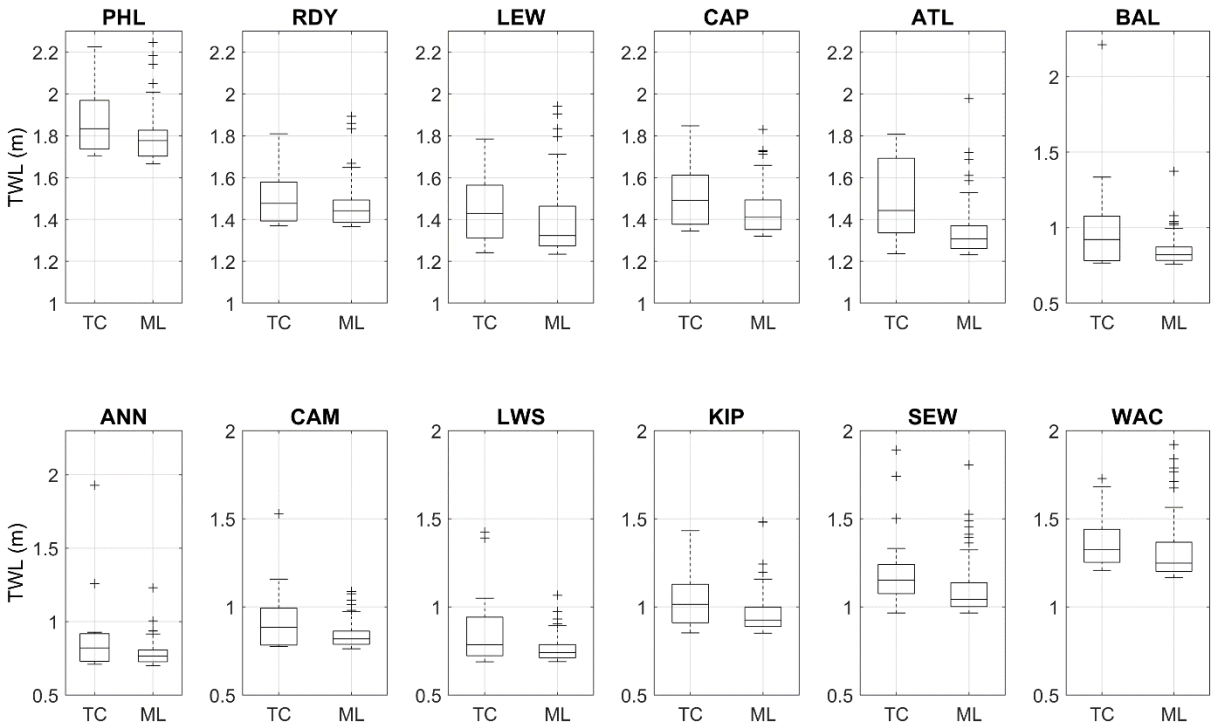

968

969

970 **Supplementary Figure 1.** Distributions of extreme total water level (TWL) due to tropical cyclones
971 (TC) and mid-latitude (ML) weather systems over 1980 – 2019. Extreme levels defined as greater
972 than 6-month return level. Box plots show medians, interquartile ranges, and maximum/minimum
973 values (hash marks) that are not considered outliers. Outliers represent data greater than 1.5 times
974 interquartile range.

975

976

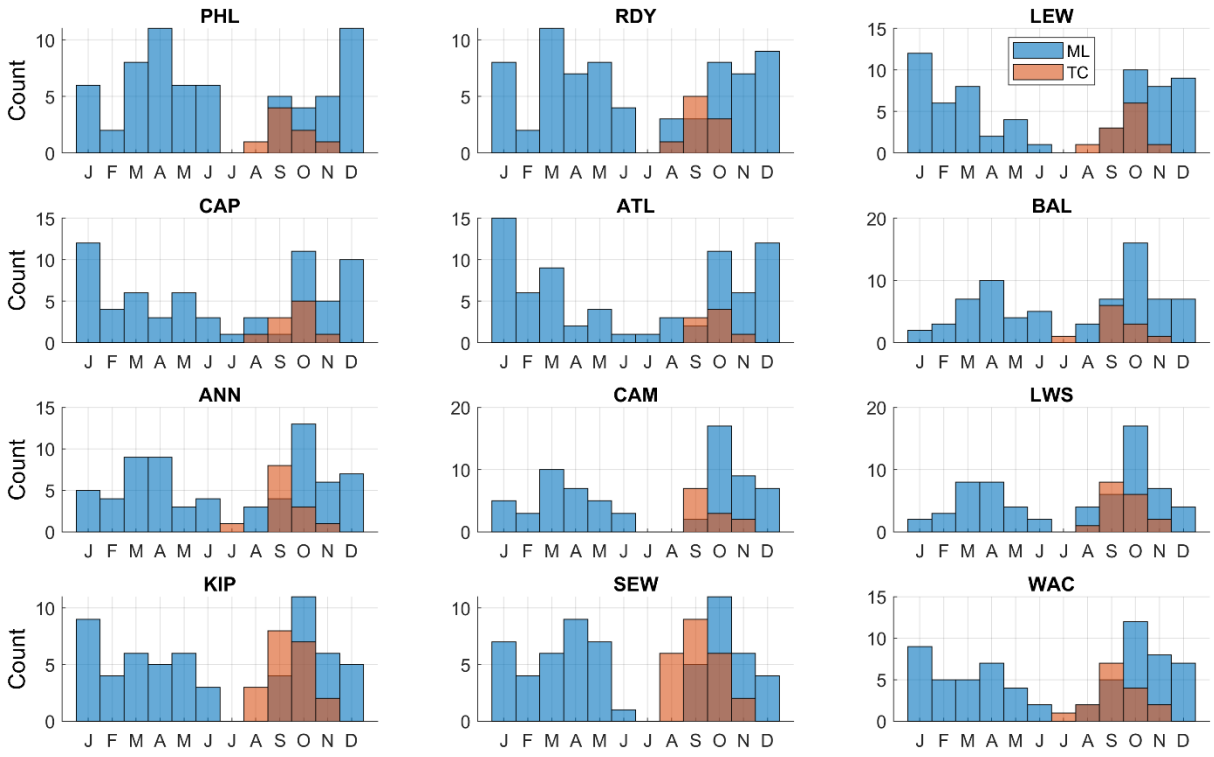

977

978

979 **Supplementary Figure 2.** Monthly frequency of occurrences of extreme total water level (TWL)
980 events due to tropical cyclones (TC, orange bars) and mid-latitude (ML, blue bars) weather systems
981 over 1980 – 2019. Extreme levels defined as greater than 6-month return level.

982

983

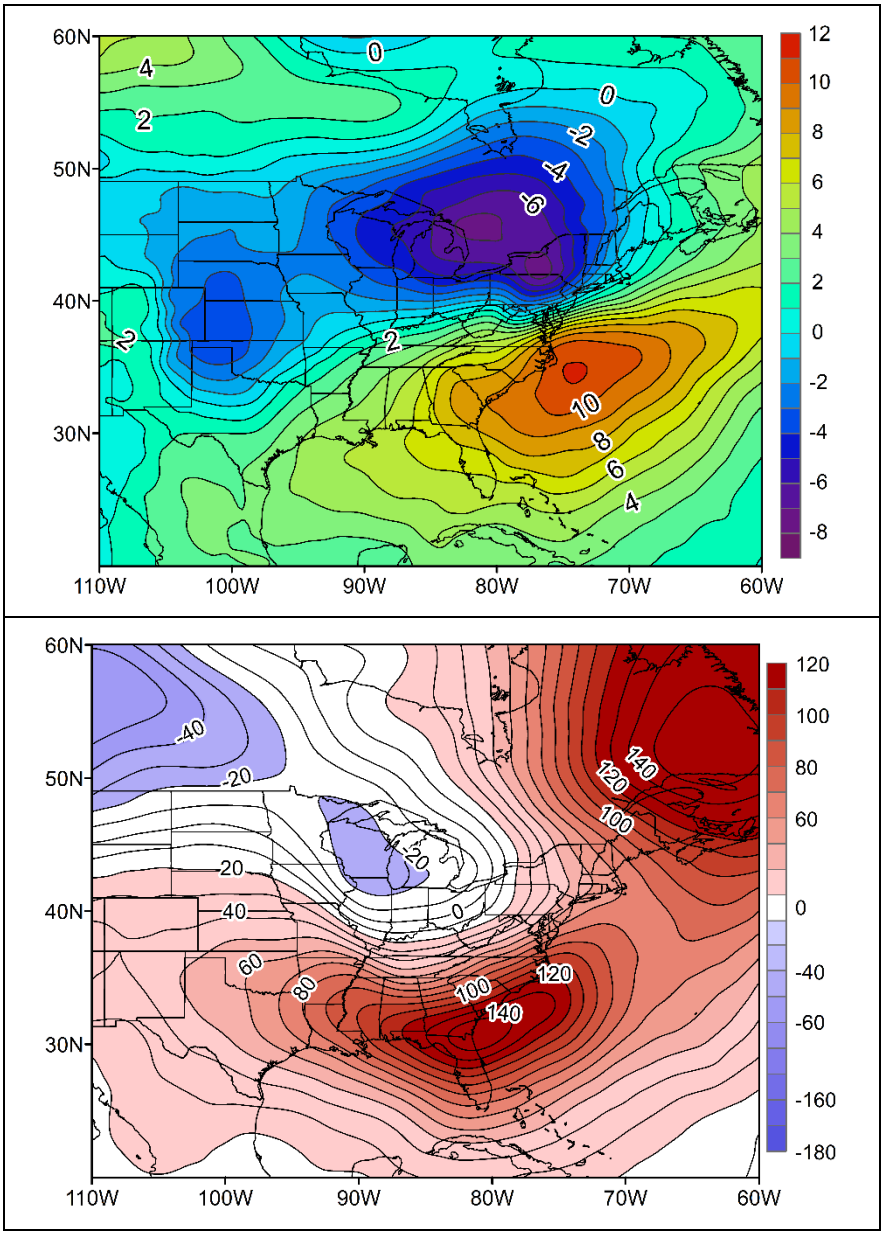

Supplementary Figure 3. Difference maps of sea-level pressure (SLP, top) and 500 hPa geopotential heights (GPH, bottom) between upper and lower Delaware Bay. Maps represent difference between mean composites of Day-0 synoptic conditions during the top 10 mid-latitude surge events over 1980 – 2019. Units of SLP and GPH difference maps are hPa and meters, respectively. Data from North American Regional Reanalysis project.

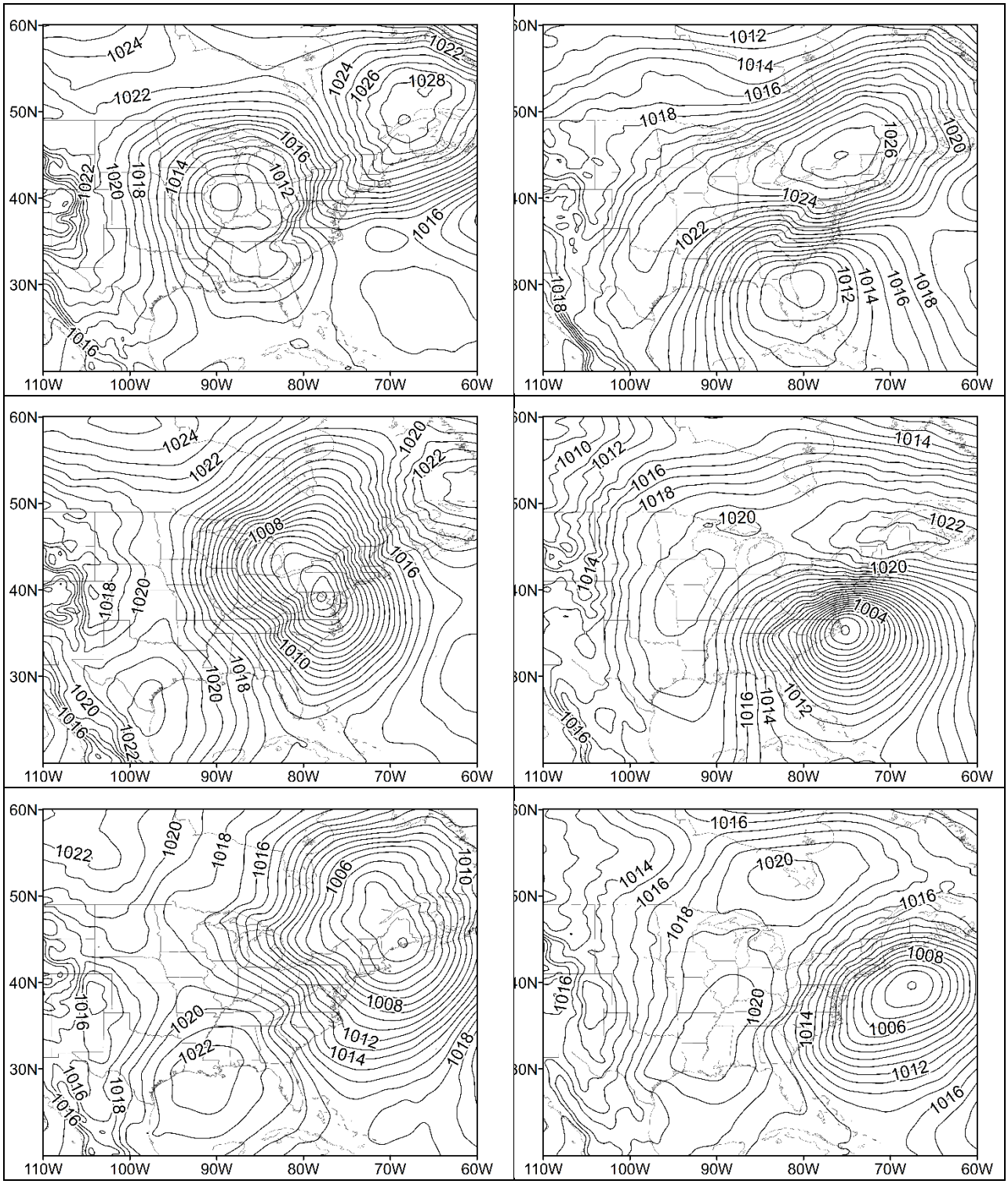

Supplementary Figure 4. Mean sea-level pressure composite maps of top 10 surge events caused by mid-latitude weather systems, for 24 hours before the event (top row), day of the event (middle row), and 24 hours after the event (bottom row). Left (right) column the upper (lower) Chesapeake Bay. Data from North American Regional Reanalysis project.

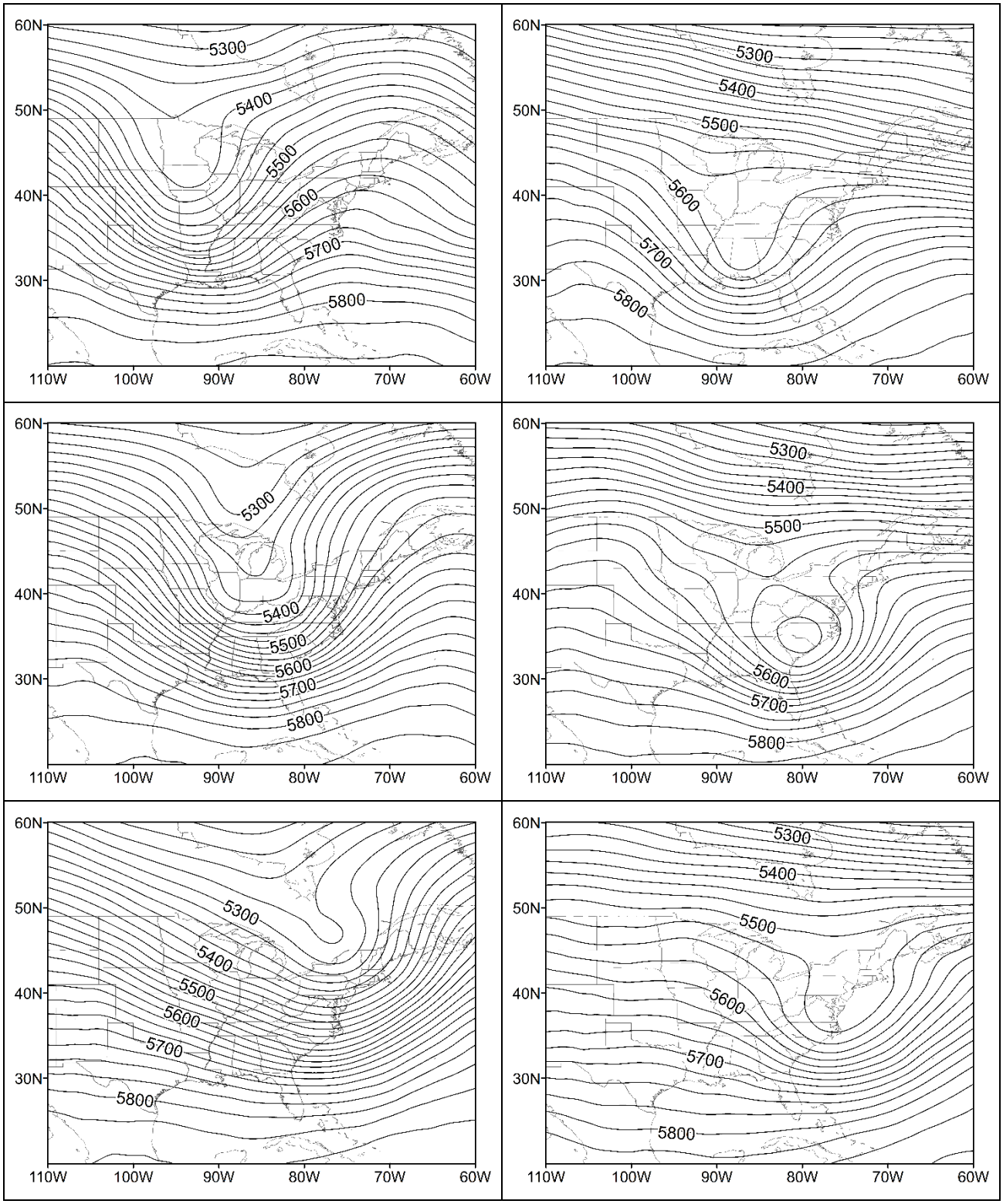

Supplementary Figure 5. Mean 500 hPa geopotential height composite maps of top 10 surge events caused by mid-latitude weather systems, for 24 hours before the event (top row), day of the event (middle row), and 24 hours after the event (bottom row). Left (right) column the upper (lower) Chesapeake Bay. Data from North American Regional Reanalysis project.

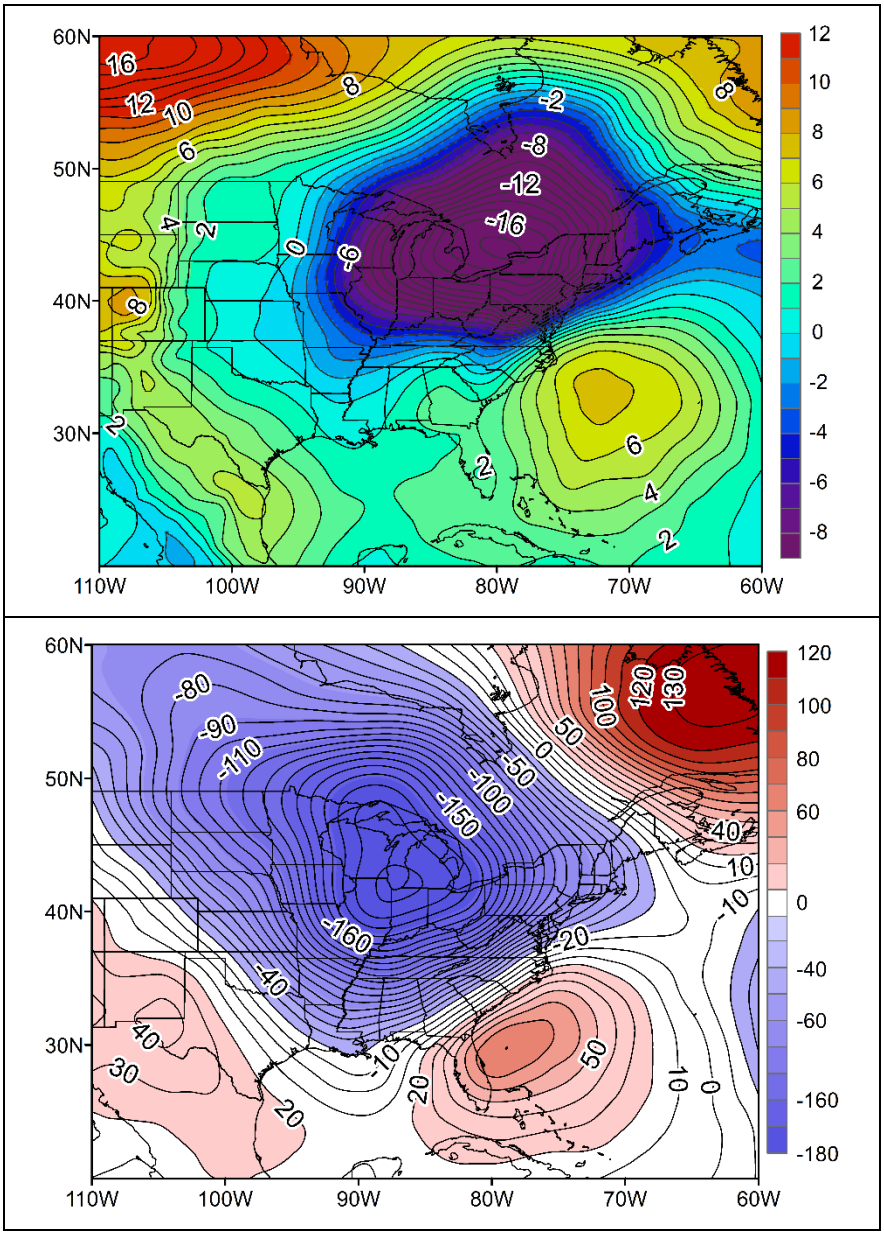

Supplementary Figure 6. Difference maps of sea-level pressure (SLP, top) and 500 hPa geopotential heights (GPH, bottom) between upper and lower Chesapeake Bay. Maps represent difference between mean composites of Day-0 synoptic conditions during the top 10 mid-latitude surge events over 1980 – 2019. Units of SLP and GPH difference maps are hPa and meters, respectively. Data from North American Regional Reanalysis project.